AD-A164 733 HIGH FREQUENCY P WAVE ATTENUATION AND DEGRADATION OF DETECTION CAPABILITY.. (U) SCIENCE APPLICATIONS INTERNATIONAL CORP SAN DIEGO CA T C BACHE ET AL. 1/1

UNCLASSIFIED 05 SEP 85 SAIC-85/1020 AFGL-TR-85-0211 F/G 8/11 NL

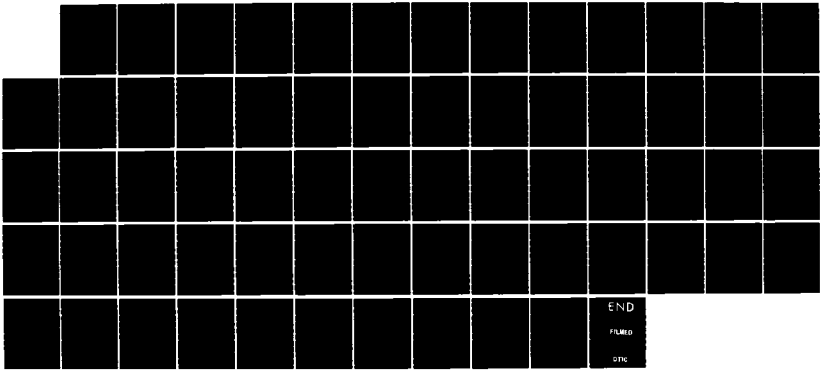

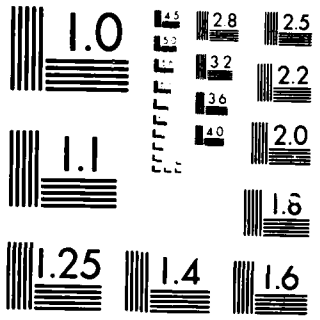

MICROCOPY RESOLUTION TEST CHART

NATIONAL BUREAU OF STANDARDS 1963-A

(9)

AFGL-TR-85-0211

AD-A164 733

HIGH FREQUENCY P WAVE ATTENUATION AND DEGRADATION OF DETECTION CAPABILITY BY LARGE EARTHQUAKES

THOMAS C. BACHE
STEVEN R. BRATT

Science Applications International Corporation
10210 Campus Point Drive
San Diego, CA 92121

September 1985

Semiannual Technical Report No. 1
December 1984 - June 1985

AIR FORCE GEOPHYSICS LABORATORY
AIR FORCE SYSTEMS COMMAND
UNITED STATES AIR FORCE
HANSCOM AIR FORCE BASE, MASSACHUSETTS 01731

CONTRACTOR REPORTS

This technical report has been reviewed and is approved for publication.

JAMES F. LEWKOWICZ
Contract Manager

JAMES C. BATTIS
Acting Chief
Solid Earth Geophysics Branch

FOR THE COMMANDER

DONALD H. ECKHARDT
Director
Earth Sciences Division

This report has been reviewed by the ESD Public Affairs Office (PA) and is releasable to the National Technical Information Service (NTIS).

Qualified requesters may obtain additional copies from the Defense Technical Information Center. All others should apply to the National Technical Information Service.

If your address has changed, or if you wish to be removed from the mailing list, or if the addressee is no longer employed by your organization, please notify AFGL/DAA, Hanscom AFB, MA 01731. This will assist us in maintaining a current mailing list.

unclassified
SECURITY CLASSIFICATION OF THIS PAGE

AD-A164733

9

REPORT DOCUMENTATION PAGE

1a REPORT SECURITY CLASSIFICATION: UNCLASSIFIED	1b RESTRICTIVE MARKINGS
2a SECURITY CLASSIFICATION AUTHORITY	3 DISTRIBUTION/AVAILABILITY OF REPORT: Approved for public release; distribution unlimited.
2b DECLASSIFICATION/DOWNGRADING SCHEDULE	
4 PERFORMING ORGANIZATION REPORT NUMBER(S): SAIC-85/1820	5 MONITORING ORGANIZATION REPORT NUMBER(S): AFGL-TR-85-0211
6a NAME OF PERFORMING ORGANIZATION: SCIENCE APPLICATIONS INTERNATIONAL CORPORATION; 6b OFFICE SYMBOL (If applicable)	7a NAME OF MONITORING ORGANIZATION: AIR FORCE GEOPHYSICS LABORATORY (LWH)
6c ADDRESS (City, State, and ZIP Code): 10210 CAMPUS POINT DRIVE, SAN DIEGO, CA 92121	7b ADDRESS (City, State, and ZIP Code): HANSCOM AIR FORCE BASE, MA 01731
8a NAME OF FUNDING/SPONSORING ORGANIZATION: DARPA; 8b OFFICE SYMBOL (If applicable): GSD	9 PROCUREMENT INSTRUMENT IDENTIFICATION NUMBER: F19628-85-C-0021
8c ADDRESS (City, State, and ZIP Code): 1400 WILSON BOULEVARD, ARLINGTON, VA 22209	10 SOURCE OF FUNDING NUMBERS: PROGRAM ELEMENT NO 61101F; PROJECT NO 5A10; TASK NO DA; WORK UNIT ACCESSION NO AB

11 TITLE (Include Security Classification)
HIGH FREQUENCY P WAVE ATTENUATION AND DEGRADATION OF DETECTION CAPABILITY BY LARGE EARTHQUAKES

12 PERSONAL AUTHOR(S)
BACHE, THOMAS C. and STEVEN R. BRATT

13a TYPE OF REPORT	13b TIME COVERED	14 DATE OF REPORT (Year, Month, Day)	15 PAGE COUNT
SEMI-ANNUAL REPORT #1	FROM DEC. '84 TO JUN. '85	1985 September 5	64

16 SUPPLEMENTARY NOTATION

17 COSATI CODES			18 SUBJECT TERMS (Continue on reverse if necessary and identify by block number)
FIELD	GROUP	SUB-GROUP	SEISMOLOGY; NUCLEAR EXPLOSION SEISMOLOGY; SEISMIC ATTENUATION; EARTHQUAKE DETECTION

19 ABSTRACT (Continue on reverse if necessary and identify by block number)

-This report describes two distinct seismological studies. The first is "High Frequency P Wave Attenuation Along Five Teleseismic Paths from Central Asia." P Wave spectra from E. Kazakhstan explosions recorded at five arrays are computed from 0.5 to 8 Hz and corrected for the source spectrum. Models for Q are constructed for all five paths using an absorption band model. The Q exhibits strong frequency dependence in the band from 0.5 to 3 Hz, and is nearly the same for all five paths. The second study is, "An Investigation of the Degradation of Teleseismic Detection Capability Caused by Large Earthquakes." A ten year global seismicity bulletin is searched to determine the extent to which large earthquakes inhibit the detection of small earthquakes occurring a short time thereafter. Significant degradation of the detection capability of the 115 station global network contributing to the bulletin is seen for periods up to an hour for earthquakes of M_b 5.8 and larger.-

20 DISTRIBUTION/AVAILABILITY OF ABSTRACT	21 ABSTRACT SECURITY CLASSIFICATION
☐ UNCLASSIFIED/UNLIMITED ☒ SAME AS RPT. ☐ DTIC USERS	UNCLASSIFIED

22a NAME OF RESPONSIBLE INDIVIDUAL	22b TELEPHONE (Include Area Code)	22c OFFICE SYMBOL
JAMES F. LEWKOWICZ	617-861-3028	LWH

DD FORM 1473, 84 MAR — 83 APR edition may be used until exhausted. All other editions are obsolete.

SECURITY CLASSIFICATION OF THIS PAGE
UNCLASSIFIED

TABLE OF CONTENTS

I	INTRODUCTION	1
II	HIGH FREQUENCY P WAVE ATTENUATION ALONG FIVE TELESEISMIC PATHS FROM CENTRAL ASIA	3
	Summary	4
	Introduction	5
	P-Wave Spectra at the UKAEA Arrays	7
	Data from NORSAR	9
	NORSAR Data Analysis	10
	Source Corrected Spectra	17
	Attenuation Models	25
	Spectra for Long Windows	27
	Discussion	29
	Acknowledgements	33
	References	34
III	AN INVESTIGATION OF THE DEGRADATION OF TELESEISMIC DETECTION CAPABILITY CAUSED BY LARGE EARTHQUAKES	36
	Introduction	37
	Data	37
	Experiment	40
	Results	44
	Earthquake Swarms	54
	Discussion	56
	Conclusions	58
	References	59

I. INTRODUCTION

This report includes two sections that describe separate seismological studies. The first (Section II) is entitled, "High Frequency P Wave Attenuation Along Five Teleseismic Paths from Central Asia." This is a manuscript which has been submitted for publication in the Geophysical Journal of the Royal Astronomical Society. It describes an analysis of P wave spectra from E. Kazakhstan explosions recorded at four United Kingdom (EKA, GBA, WRA and YKA) arrays and the NORSAR array. The spectra are stacked across the array and for many explosions in the same part of the test site. They are then corrected for the source spectrum. In this way we obtain spectra that essentially display the effect of attenuation. The attenuation effect appears to be nearly the same for all five paths in the 0.5 to 3 Hz band. From 3 to 8 Hz the four paths to the United Kingdom arrays are nearly the same, but the NORSAR path is quite different in that the source-corrected spectrum is nearly flat. This means that the path average Q is nearly proportional to frequency in this band. Models for Q are constructed for all five paths using an absorption band model to match the low frequency behavior. For the paths to the United Kingdom arrays we superimpose a second Q that is essentially independent of frequency above 3 Hz to match the high frequency behavior. This apparently represents amplitude attenuation primarily by scattering.

Section II is entitled, "An Investigation of teh Degradation of Teleseismic Detection Capability Caused by Large Earthquakes." It describes an analysis of a ten-year global sesimicity bulletin constructed by Ringdal (1984) by reprocessing ISC Bulletin data from a network of 115 stations selected for their distribution and consistent reporting. Maximum likelihood m_b were computed for all 74000 events in this bulletin. Our objective is to estimate the extent to which large earthquakes inhibit the detection of small earthquakes. This is done by comparing the number of earthquakes detected immediately after large earthquakes to the number expected, based on average seismicity over the ten-year period. Aftershocks of the large earthquakes are deleted.

The results show that the detection capability of this 115 station network is significantly degraded for periods up to an hour or more for earthquakes as small as m_b 5.8. During these periods fewer than 80% of the events expected with $m_b < 4.5$ are detected. There appears to be little or no effect on the capability to detect events with $m_b > 4.5$.

The motivation for this study is to develop some empirical basis for assessing the effectiveness of the "Hide-in-Earthquake" (HIE) scheme for evading detection of a clandestine nuclear test. Taken alone, these results add marginally to such an assessment. One reason is that effects of the large earthquakes are only seen for events with m_b below the 90% incremental detection threshold (m_b 4.46) of the bulletin, so the number of events that fail to be detected due to network deficiencies is usually larger than the number hidden by signals from large earthquakes. Another reason is that this experiment demonstrates that small earthquakes can be hidden by larger earthquakes, but explosion signals from events of the same size have characteristics that may make them easier to detect. Some theoretical analysis involving simulations is necessary to quantitatively assess the likely effectiveness of the HIE scenario. The greatest value of these results is most likely to be in providing a basis for normalizing simulations to actual network performance.

SECTION II

HIGH FREQUENCY P WAVE ATTENUATION ALONG FIVE TELESEISMIC PATHS FROM CENTRAL ASIA

Thomas C. Bache
Science Applications International Corporation
10210 Campus Point Drive
San Diego, California

Steven R. Bratt
Science Applications International Corporation
10210 Campus Point Drive
San Diego, California

Hilmar Bungum
NTNF/NORSAR
P.O. Box 51
N-2007
Kjeller, Norway

Summary

A model for the attenuation of high frequency (0.5-8 Hz) P waves is developed for teleseismic paths from eastern Kazakhstan to five seismic arrays. Four are the UKAEA arrays in Scotland (EKA), Canada (YKA), India (GBA) and Australia (WRA) and the attenuation effects on these paths were studied in an earlier paper (Bache et al., 1985). Here we add the path to NORSAR (Southern Norway) and extend the analysis by introducing explicit corrections for the source spectrum. The events are underground explosions at the Soviet Semipalatinsk test site and the source corrections are based on the Mueller and Murphy (1971) model which is normalized to U.S. experience. Averaging spectra from many array elements and many explosions leads to smooth spectra that essentially display the effects of attenuation on each path. There are three major features. First, from 0.5 to 3 Hz the attenuation effects are nearly the same for all five paths and indicate strong frequency dependence in Q. Second, from 3 to 8 Hz the four UKAEA paths are nearly the same, but the NORSAR path is quite different in that the source-corrected spectrum is nearly flat. This means that the path-average Q is nearly proportional to frequency in this band. Finally, above 7-8 Hz some additional attenuation effects are seen in the NORSAR data. Thus, for this teleseismic P wave path the maximum signal/noise occurs at 7 or 8 Hz. The attenuation effects from 0.5 to 8 Hz can be represented with absorption band models. For the paths to the UKAEA arrays the preferred model has t_0^* (travel time/Q at long period) about 0.6 seconds and τ_m about 0.05 seconds. Superimposed on this is a frequency-independent t_1^* of about 0.1 seconds. This dominates the high frequency ($f > 3$ Hz) attenuation and appears to represent attenuation primarily by scattering. For the NORSAR path a single absorption band ($t_0^* \simeq 0.7$, $\tau_m \simeq 0.045$) is adequate for the 0.5 to 7 Hz band. We have no explanation for why this path is so different, but it appears to be associated with some difference in the contribution of scattering

to the attenuation of the initial P wave.

Introduction

Regional attenuation variations are important because they cause systematic variations in seismic wave amplitudes. For short period P waves these amplitude variations are very difficult to see in the amplitude (or m_b) data because there are much larger amplitude variations due to elastic effects. This is best seen in data from the large arrays like LASA (Chang and Von Seggern, 1980) and NORSAR (Ringdal and Husebye, 1982). However, attenuation or Q is a dominant factor controlling the shape of short period P wave spectra. Thus, spectral shape variations have been used to map regional attenuation variations (Der et al., 1982, 1985). It is somewhat easier to determine the differences between paths than to determine the average-path Q on any particular path because of tradeoffs with other factors (especially the source spectrum).

Our objective is to estimate the average-path Q on five teleseismic paths, using the spectrum of short-period P waves from underground nuclear explosions. The frequency band is 0.5 to 8 Hz and the paths are from the Soviet test site in eastern Kazakhstan to the four United Kingdom Atomic Energy Authority (UKAEA) arrays and the NORSAR array in southern Norway. The advantage of data from arrays is that recordings from the individual elements can be stacked to suppress uncorrelated noise and signal features due to near-receiver structure. When the sources include many similar events (such as underground nuclear explosions within a test site), the event spectra can be averaged to suppress uncorrelated source region effects. The result of such a double-averaging process is a P-wave spectrum shaped almost entirely by attenuation effects and the mean source spectrum. For underground nuclear explosions the source spectrum is rather simple and can be assumed to be a proportional to f^{-2} above the source corner frequency (e.g., Mueller and Murphy, 1971; von Seggern and Blandford, 1972). This corner frequency usually occurs at frequencies from 1 to 3 Hz,

depending on the explosion yield and depth and on properties of the near source geology. Thus, when the corner frequency is known, an average path spectrum can be computed that essentially displays the effect of attenuation.

The medium aperture UKAEA arrays EKA (Scotland), YKA (Canada), GBA (India) and WRA (Australia) are especially useful for computing average path spectra for high frequency P waves because of the array design (element spacings of 1 to 2.5 km) and the seismometer response (essentially flat to velocity for frequencies above 2 Hz). Bache et al. (1985, hereafter called Paper I) computed P wave spectra at these four arrays for a large suite of E. Kazakhstan explosions and determined a Q model for these paths. In this paper we extend the analysis of Paper I by introducing explicit source corrections, and also by adding the path to NORSAR.

Unfortunately, NORSAR data are not nearly as well-suited for this purpose as the UKAEA array data. The relatively short operating history of NORSAR, the clipping levels, and the frequency response of the system all act to reduce the number of useful data. Nevertheless, there are adequate data to demonstrate that this path is quite different from the paths to the UKAEA arrays for frequencies above 3 Hz. In particular, the NORSAR recordings are extraordinarily rich in high frequency energy. Below 3 Hz the effect of attenuation is quite similar on all five paths.

In this paper we first summarize the key results for the four E. Kazakh-UKAEA array paths from Paper I. We then analyze the spectra for NORSAR recordings of some of the same E. Kazakh events and introduce source corrections so attenuation effects are isolated for all five paths. The epicentral distance to NORSAR is about 38 degrees, so those P waves penetrate to a depth of about 900 km. The epicentral distances to the UKAEA arrays range from 36 (GBA) to 85 (WRA) degrees, so the penetration depths range from about 850 to 2500 km. The apparent attenuation effects on these five paths are compared and interpreted in

terms of an average-path Q model. As an important byproduct of this study, we also consider the signal-to-noise characteristics of explosion P-waves recorded at NORSAR.

P-Wave Spectra at the UKAEA Arrays

In Figure 1 average path spectra are plotted for paths from the eastern Kazakhstan test site to the four UKAEA 20-element arrays. These are computed in the following way. For each element seismogram energy density spectra are computed for very short (typically 2.2 to 2.5 seconds) time windows isolating the first arriving compressional wave. The power spectrum of a 3.8 second noise window just before the signal is subtracted from this energy density spectrum. The Fourier spectrum for the event is then computed from the average of these "corrected" energy density spectra for all elements of the array. This gives a more accurate estimate for the high frequency signal energy than the spectrum of an array beam, since beaming suppresses incoherent high frequency signal energy. Also, Paper I shows that if the noise is stationary and uncorrelated with the signal, its contribution to this spectral estimate diminishes as the number of elements increases. The final step is then to average spectra from similar events in a small source region to suppress uncorrelated source effects.

The spectra obtained this way (e.g., Figure 1) are quite smooth and are almost entirely shaped by the average source spectrum and the effect of attenuation along the path. Accurate attenuation estimates depend on accurate corrections for the source, which is more straightforward for underground explosions than for earthquakes. For both, the source spectrum for the direct P wave should be roughly proportional to f^{-n} above some corner frequency. There remains some controversy about the value of n for explosions, but most of the evidence supports $n = 2$, and we shall see that the NORSAR spectra appear to confirm that value. The total source spectrum is modulated by interference between the direct and reflected (mainly from the surface) phases, and modified by any energy added by secondary sources (such as the triggered release of

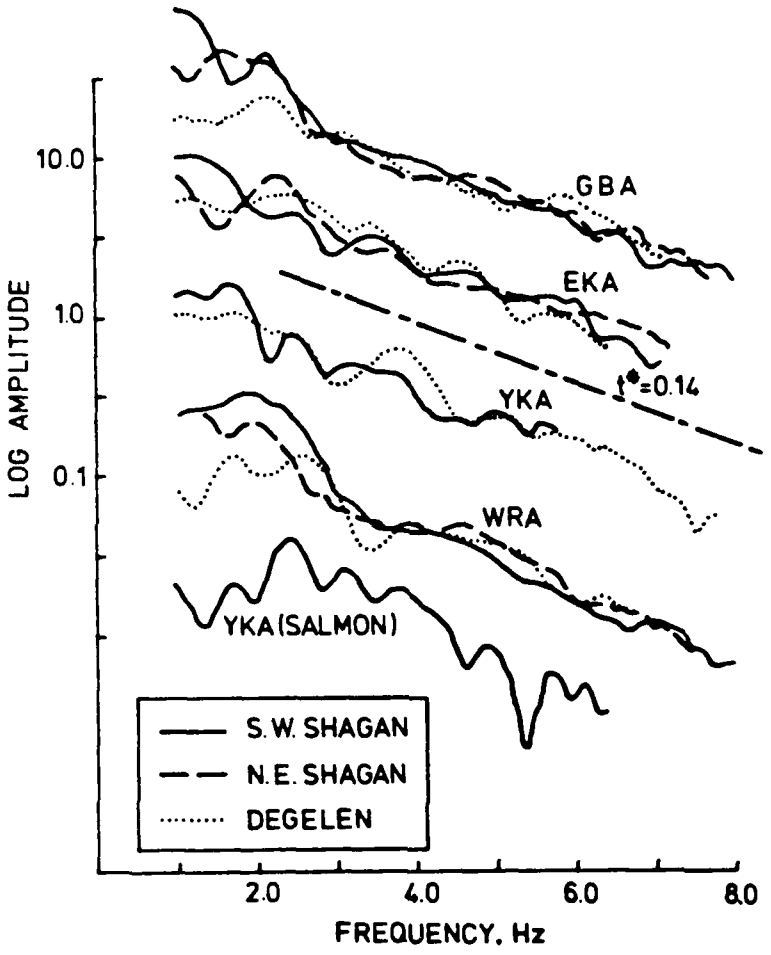

Figure 1 Path-average spectra are shown for the paths from the Soviet E. Kazakhstan test site to the United Kingdom Atomic Energy Authority (UKAEA) arrays. Also shown is the spectrum for the US SALMON event at YKA and a line with slope corresponding to $t^* = 0.14$ (reproduced from Bache et al., 1985).

stored tectonic stresses) that may occur.

All spectra shown in Figure 1 have been multiplied by f^2 to correct for the source. Spectra plotted this way should decrease with decreasing frequency below the corner frequency where the f^2 correction is invalid. This is exemplified by the spectrum for SALMON, which is known to have a corner frequency near 3 Hz (Springer et al., 1968). Thus, the highest corner frequencies occur for the Degelen explosions, and the lowest for the explosions in S.W. Shagan.

The explosions included in the spectra shown in Figure 1 are listed in Paper I. Except at YKA (where data are few because $m_b > 5.5$ events are clipped), they are divided into three populations representing different portions of the eastern Kazakhstan test site. The total number of explosions processed at each station is 37(EKA), 36(GBA), 28(WRA) and 16(YKA). Therefore, about 1800 individual seismograms are represented in the figure.

Data from NORSAR

Since 1976, the NORSAR array has consisted of seven subarrays spread over an area of about 3,000 km^2. Each subarray has six vertical short period seismometers spaced about three km apart. Between 1971 and 1976 the array was much larger and included 22 subarrays (Ringdal and Husebye, 1982). The standard digital sampling rate is 20/second and the displacement response of the standard instrumentation increases faster than frequency up to 4.75 Hz. At that point a strong anti-aliasing filter (18 dB/octave) is applied. Since the maximum resolution of the digitization (0.0427 nm/count) covers only 42 dB (an additional 36 dB is provided by gain ranging), signal spectra cannot be recovered with confidence for frequencies much above 5 Hz (Bungum et al., 1975). However, beginning in 1978, one seismometer at each subarray was altered so the response continues to increase to 8 Hz where the 18 dB/octave filter is applied. The sensitivity to 8 Hz is thereby increased by a factor of 10. The results to be presented are

from these "8 Hz" instruments.

The data are recordings of the explosions listed in Table 1. Marshall et al. (1984) computed locations and m_b (including station corrections) for most of them. Nearly all are in the Degelen Mountain portion of the test site (near 49^oN 78^oE). Also listed in the table are the ISC m_b and the number of 8 Hz instruments that provided usable data. Events larger than those listed are clipped on all channels. For the last explosion on the list (30 May 1983) the data were logged on two separate systems. In addition to the standard 20 sample/second recording, the data were digitized at 62.5 samples/second on a Kinemetrics PDR-2 system, adding an additional 42 dB amplification. Also, the anti-alising filter was moved to 25 Hz (see Bungum et al., 1985, for details). Our conclusions about signal spectra above 10 Hz are based on the recordings of this explosion.

The first six explosions in Table 1 are among those processed in Paper I. Typical NORSAR seismograms are shown in Figure 2. Single elements of the UKAEA arrays record superficially similar waveforms for these explosions.

NORSAR Data Analysis

The spectra computed from five 8 Hz seismometers for two of the larger explosions in Table 1 are shown in Figure 3. Also shown is the noise spectrum computed from the average noise power (based on a 3.8 second sample of noise before the signal on each element). The properties of the noise at NORSAR and surrounding areas have been carefully studied for frequencies up to 40 Hz (Bungum et al., 1985). At quiet sites (i.e., no local noise sources) the noise (P_N) is represented by the line $\log P_N \propto -5 \log f$, with $P_N = 10^{-23}$ m^2/Hz. The Fourier spectrum equivalent (correcting for normalization by the sample window length) of that noise model is plotted, and agrees well with these samples.

The signal spectrum is nearly flat from 3 to beyond 7 Hz when plotted

TABLE 1

EASTERN KAZAKHSTAN EXPLOSIONS

EVENT	DATE	ISC M_b	MARSHALL *et al* m_b	ELEMENTS
1	26 March 1978	5.6	5.61	4
2	22 April 1978	5.3	5.28	5
3	28 July 1978	5.7	5.66	3
4	31 October 1978	5.2	5.22	5
5	31 May 1979	5.3	5.24	3
6	18 October 1979	5.2	5.19	3
7	14 December 1978	4.8	4.71	4
8	20 December 1980	4.7	4.67	5
9	30 November 1979	4.5	4.47	5
10	26 December 1980	4.5	4.25	2
11	27 May 1981*	5.5	5.46	2
12	20 September 1978**	4.3	--	4
13	30 May 1983	>5	--	2

*Shagan River area near 50°N 79°E

**Konystan area near 50°N 78°E

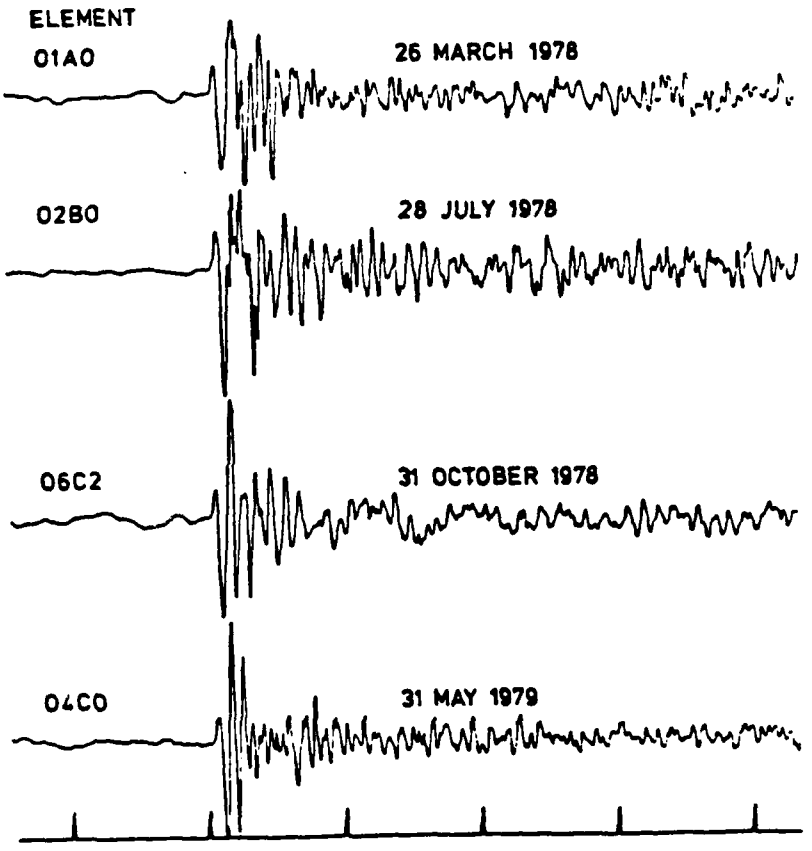

Figure 2 Recordings of four Degelen explosions (Table 1) are plotted from subarray elements with 8 Hz seismometers. The subarray identification is as in Ringdal and Husebye (1982). The time marks are at 5 second intervals.

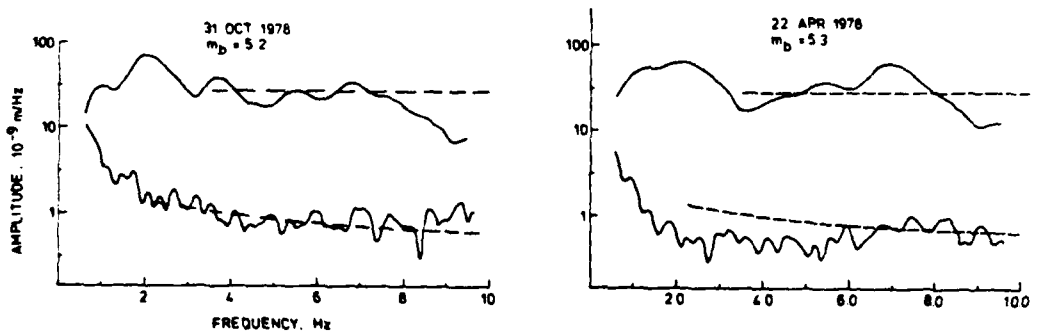

Figure 3 The spectra for two of the events of Table 1 are shown together with the average noise in a window just before the P onset. A horizontal dashed line is sketched through each signal spectrum and the NORSAR noise model of Bungum et al. (1985) is sketched through the noise.

with the f^2 source correction. The spectra for the other Degelen events with $m_b \geq 5.2$ look much the same as is demonstrated in Figure 4. These are very different from the spectra for the four paths in Figure 1, which all decay at a nearly constant rate above 3 Hz. For the path to NORSAR the apparent attenuation has almost no frequency-dependent effect between 3 and 7 Hz. Since attenuation cannot be negative, spectra like this confirm that the source spectrum decays no faster than f^{-2} above the corner frequency. The only other possibility is that the explosion is accompanied (nearly simultaneously) by small energetic earthquakes with corner frequencies near 8 Hz. But the results in Figure 1, especially their consistency for events in different areas, seem to rule this out.

Near 7 Hz the signal/noise is a factor of 30 or so for these events, and is clearly decreasing above 8 Hz. This suggests that the capability to detect small events might be enhanced by designing the instrumentation to emphasize frequencies around 7-8 Hz, rather than the much lower frequencies that dominate the seismograms from current instrumentation. To further explore this question, we need to examine spectra from smaller events and higher sampling rate instrumentation.

In Figure 5 we show the spectra for events 7-12 in Table 1. Four are smaller Degelen explosions and two are explosions in other parts of the eastern Kazakhstan test site. Various combinations of elements were available for computing these spectra, so in that sense the computations are not entirely consistent. The four Degelen spectra are similar to those in Figure 3. The only significant difference is at low frequency where the smaller m_b event spectra behave as expected for higher source corner frequency. The maximum signal/noise occurs around 7 Hz and decreases at higher frequencies. For the explosions at Konystan and Shagan River the signal spectrum does not decay so obviously above 7-8 Hz. It is difficult to know whether this is a general feature without data from more events. However, the maximum signal/noise still occurs near 7 Hz because the noise is increasing (that is, the noise is falling off at a rate less than f^{-2}).

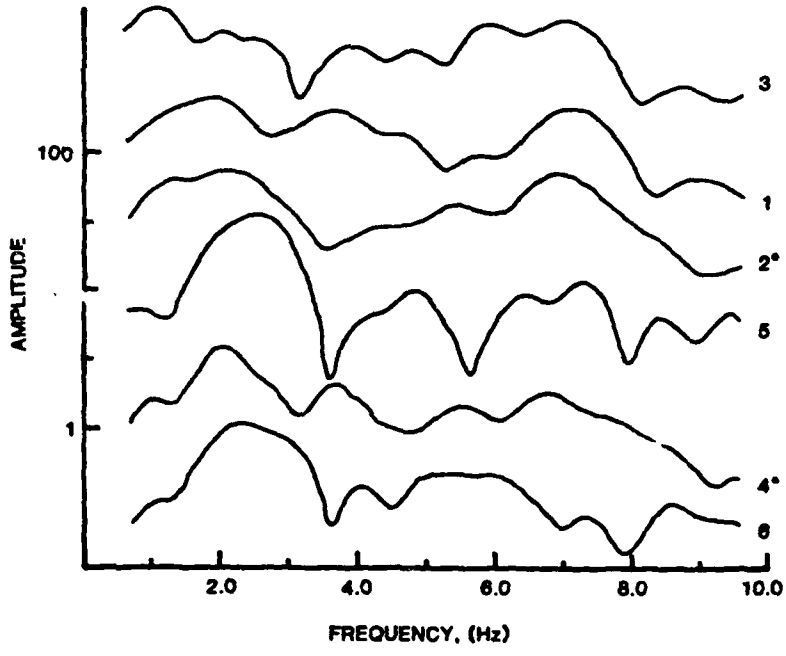

Figure 4 P wave spectra are plotted in order of ISC m_b for the first six Degelen explosions in Table 1. The number at the right is the event number in the table and the asterisk marks the two spectra repeated from Figure 3. All have been multiplied by f^2. The position with respect to the amplitude scale is arbitrary.

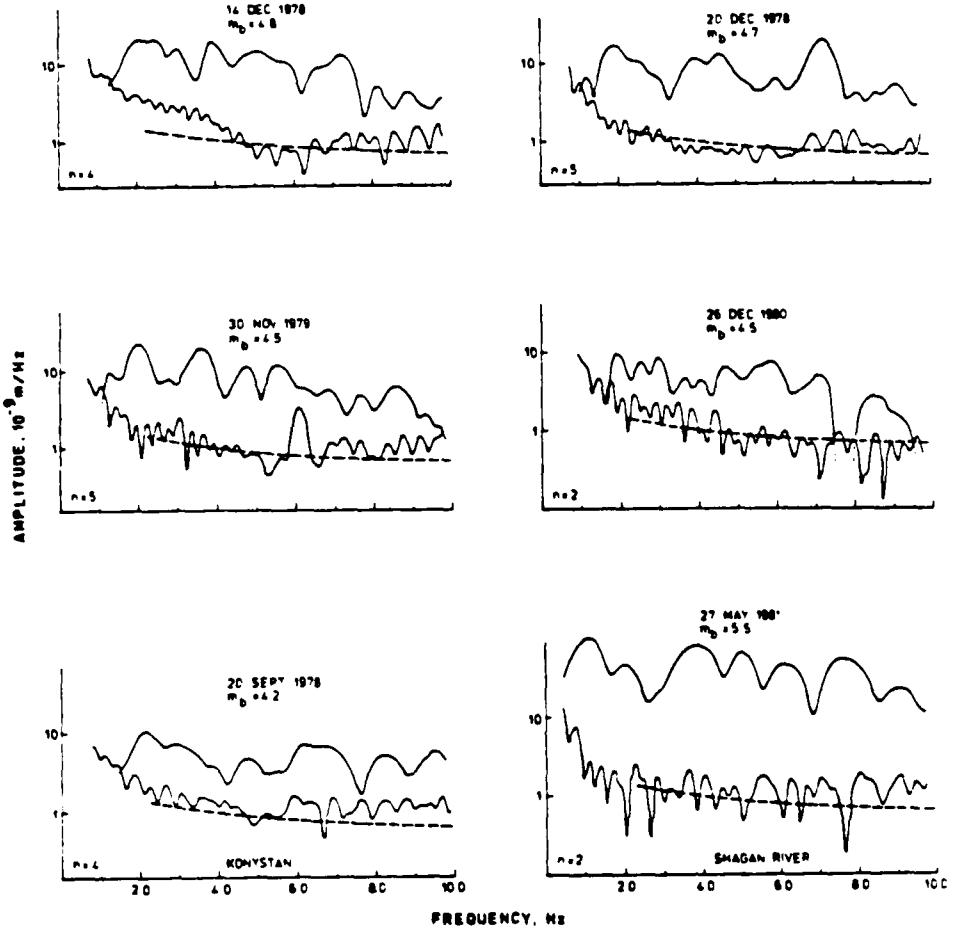

Figure 5 Spectra are plotted for six events in the same format as Figure 3. The top four are Degelen explosions and the bottom two are explosions in other portions of the eastern Kazakhstan test site.The number of elements included in the spectrum is indicated by n.

The 30 May 1983 Degelen explosion was recorded on two 8 Hz seismometers in subarray 01A, one at the surface and the other one at the bottom of a 60 m deep borehole at the same location. The output of these seismometers was digitized in the usual way (20 Hz) and was also digitized at 62.5 samples/second by the PDR-2 system (Bungum et al., 1985). Comparison of spectra from the two systems, (Figure 6) demonstrates that NORSAR spectra like those in Figures 3-5 are unbiased to near the Nyquist frequency of 10 Hz. Also, the spectrum for this Degelen explosion is similar to the others shown earlier. At the bottom of Figure 6 we plot this spectrum to 20 Hz. It decays with a nearly constant slope above 7 Hz and is lost in the noise by 12 Hz.

Source Corrected Spectra

Three major features of these spectra determine the attenuation model for the E. Kazakh-NORSAR path. First, at low frequencies they are influenced by source corner frequency effects, and a correction for them must be introduced. Second, the source-corrected spectra are essentially flat in the band between 3 and 7 Hz. The third feature, the spectral decrease above 7-8 Hz, is less well-defined since we have only one good observation of it (Figure 6). However, we note that the line representing $t^* = 0.14$ is a reasonable approximation for the rate of decay, and that this line closely follows the spectral slope above 2.5 Hz for the four paths to the UKAEA arrays (Figure 1).

To interpret the NORSAR spectra in terms of an attenuation model we need to add information developed from the much larger data base from the UKAEA arrays. The Q models for the paths from E. Kazakhstan to the UKAEA arrays given in Paper I were fit to spectra which had no explicit source correction. Rather, the Q models were fit to a subset of events for which the f^2 source correction appeared to be valid for frequencies above 1.5-1.8 Hz. Some allowance was made for the expected source effect at lower frequencies. However, for the small Degelen events in our NORSAR data base we cannot do this very convincingly because source

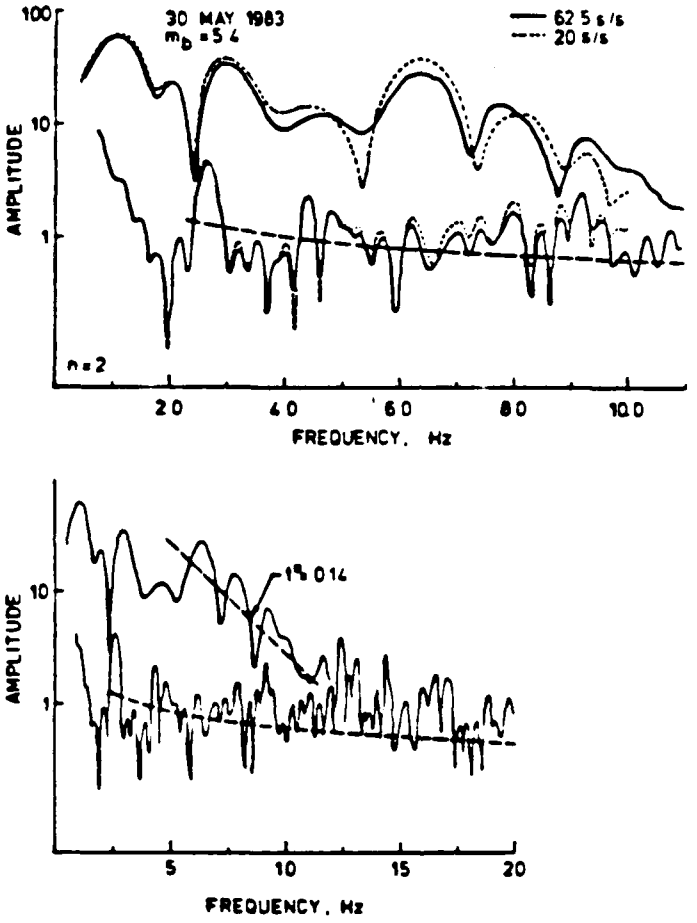

Figure 6 Signal and noise spectra are plotted for Degelen explosion recordings digitized at two different sampling rates. The higher sampling rate spectra are compared to the lower rate spectra (top) and are then replotted on a different frequency scale (bottom). On the bottom plot a line with slope corresponding to $t^* = 0.14$ is drawn through the high frequency portion of the signal spectrum.

corner frequency effects can be seen up to 3 Hz. Thus, we introduce a source correction and use the full suite of data to develop confidence in its validity.

A substantial effort has been made to determine the characteristic source spectrum for underground nuclear explosions (e.g., see the review by Bache, 1982). Analytical formulations have been suggested by many authors including Haskell (1967), Mueller and Murphy (1971), von Seggern and Blandford (1972), and Helmberger and Hadley (1981). It appears that current ideas about the explosion source spectrum and its dependence on yield and burial depth are best represented by the Mueller and Murphy (1971) source potential (Murphy, 1977; Bache, 1982), so we will use it to make the source corrections. However, we should note that the empirical validation of the Mueller-Murphy source has been mainly with data from explosions in the volcanic rocks at the Nevada Test Site. Also, the scaling laws are better constrained than the absolute amplitude and corner frequency at any particular depth and yield.

There is a strong tradeoff between source corner frequency and attenuation effects on the spectrum, particularly when the effective Q is frequency dependent. We assume that the source spectrum is the same at all stations for each event. Then the range of admissible source spectra is constrained by assuming that the attenuation effects are the same for all events on a particular path. This assumption effectively constrains the scaling of the corner frequency when we have events over a large range of m_b (i.e., yield).

We have tested various choices for the source spectrum and its scaling using the large set of UKAEA data described in Paper I. We find that good results are obtained with source spectra that scale as indicated in Figure 7. Shagan River explosions are represented by the Mueller-Murphy granite source which is scaled by assuming that m_b 6.0 corresponds to a yield (W) of 150Kt, that $m_b \propto 0.9 \log W$, and that the depth is 122 $W^{1/3}$ meters. The absolute yield and depth values have

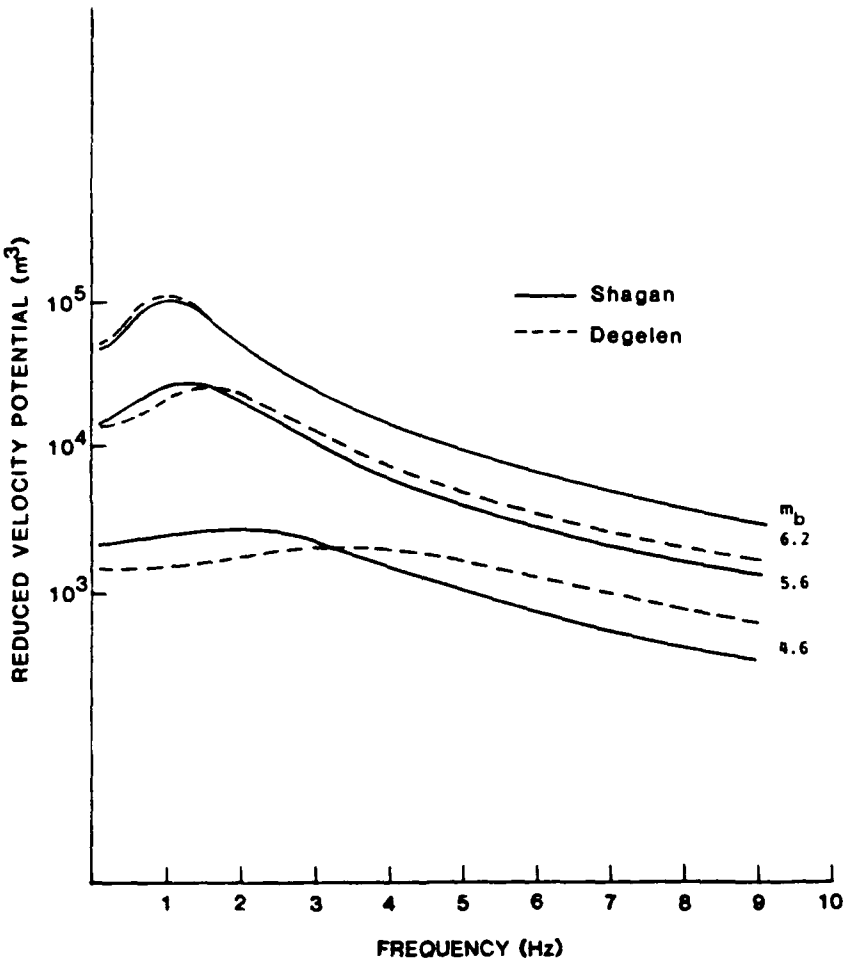

Figure 7 The reduced velocity potential (RVP) spectra used to correct for the source contribution to the observed P wave spectra are shown for three m_b values. The RVP is proportional to the far-field displacement (von Seggern and Blandford, 1972). While the plot shows actual RVP amplitudes, the corrections are made without reference to the amplitude, and only the spectral shape is important.

significance only to the extent that the Mueller-Murphy source accurately represents explosion coupling to seismic waves in the Shagan River geology. It is primarily the spectral shape and its dependence on m_b that are constrained by these data. The peak amplitude and corner frequency (f_c) scale with $W^{-0.19}$; that is, log $f_c \propto -0.21\ m_b$. The events in the Shagan River data set have $6.2 \geq m_b \geq 5.3$ (Paper I), and the spectral characteristics at low frequency clearly depend on m_b. The assumed scaling successfully removes most of these differences.

The Degelen events recorded at the UKAEA arrays have $6.0 \geq m_b \geq 5.1$. We assume that the apparent attenuation effect is the same for the Degelen and Shagan River data. Source models with frequencies that cube-root scale ($f_c \propto W^{-1/3}$; that is, log $f_c \propto -0.37\ m_b$) appear to be more consistent with the Degelen data than models (like that used for Shagan River) which have weaker m_b scaling. In the context of the Mueller-Murphy model, cube-root scaling implies that the explosions are at nearly the same depth of burial. In particular, the assumptions are the same made for Shagan River, except that the depth is fixed at 650 meters, the value chosen for m_b 6.0 events at Shagan River. Then Degelen events with $m_b < 6.0$ have higher corner frequencies than Shagan River events with the same m_b. For example, at m_b 5.4 the Degelen corner frequency is 25% higher. If the characteristic Degelen depth of burial is less than that for an m_b 6.0 event at Shagan River, this implies that there are some material property differences between the two sites (e.g., the corner frequency is expected to be higher for higher strength materials).

The source correction and stacking procedure are illustrated in Figure 8 for the GBA recordings of S.W. Shagan and Degelen events. When the spectra are plotted as in the left panel, the low frequency behavior changes with m_b as it should if the source corner frequency were decreasing with increasing m_b. The m_b for several events is indicated in the figure to illustrate this. The source corrections (Figure 7) also multiply the spectra by f^2 above the source corner frequency, but

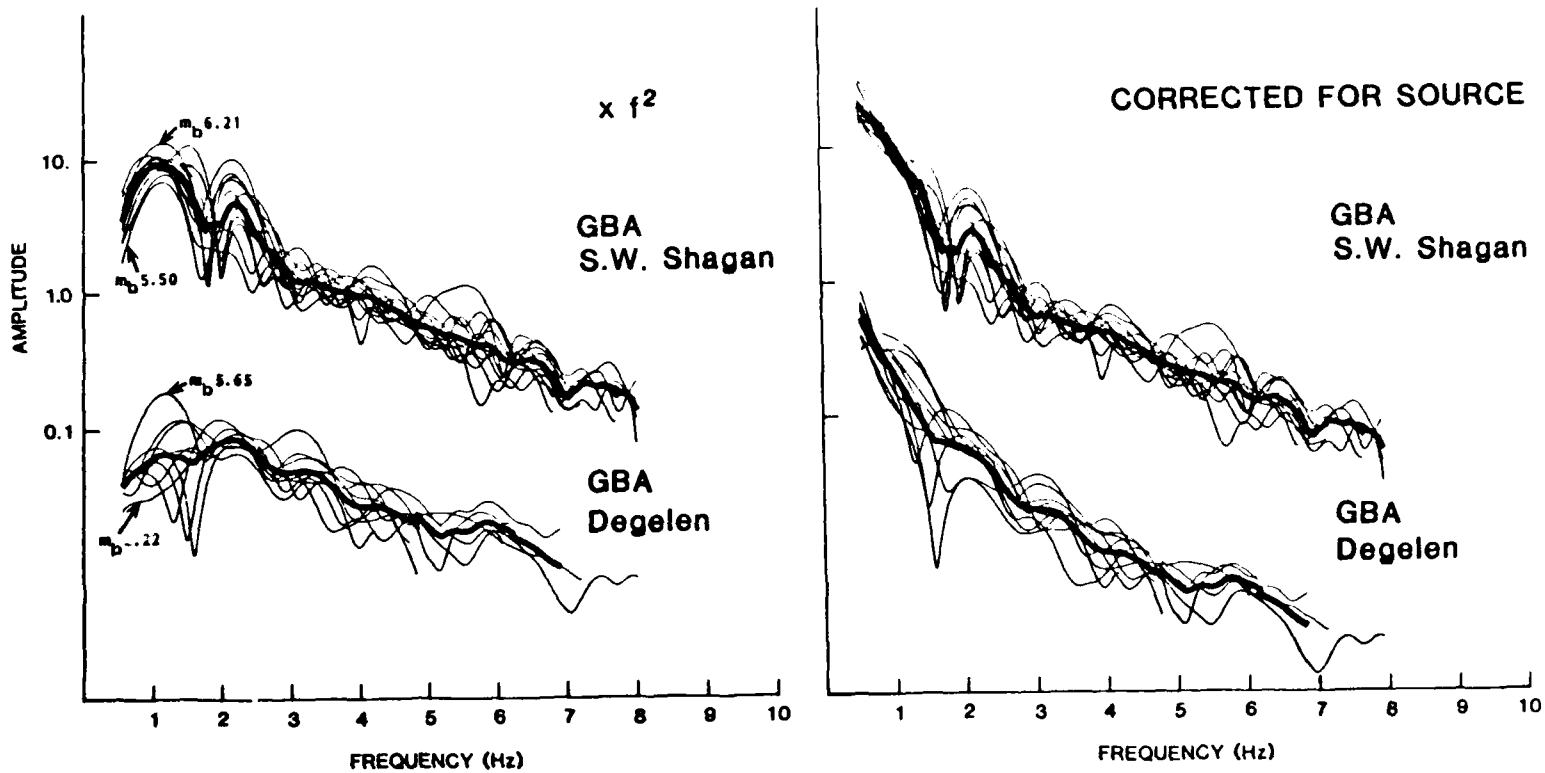

Figure 8 The source corrections and stacking procedure are illustrated for two typical event populations. All spectra in the left panel have been multiplied by f^2, while those in the right panel have been corrected by source functions scaled to the event m_b (Figure 7). The m_b corresponding to a few spectra are indicated. All spectra in each population have been shifted to have the same average amplitude (defined by a line fit by least squares) in the center of the frequency band. The heavy line is the mean spectrum for that population.

because they depend on m_b, substantially reduce the spectral variations at low frequency.

The source-corrected path spectra are plotted for all event populations being considered in Figure 9. The right panel in Figure 8 illustrates how each of these is calculated. The mean and sample standard deviation is calculated at each frequency, assuming no error in the event spectra. But since each event spectrum is an average of up to twenty array element spectra, this error should be small. Ignoring this approximation, the 95% confidence limits on the mean spectra in Figure 9 vary from 1.05 times the standard deviation (which is plotted) for the smallest set (n=6) to 0.60 times the standard deviation for the largest set (n=14).

The source-corrected path spectra in Figure 9 essentially display the effects of attenuation on these five paths. There are some modulations, presumably due to source (e.g., pP) and path effects, but the spectra are generally quite smooth and consistent. The apparent attenuation effects are essentially the same for all three portions of the E. Kazakh test site, as they should be (Figure 9a). An interesting result is that the attenuation effect is remarkably similar for the paths to all four UKAEA stations (Figure 9b-d). In Paper I the effective attenuation on these paths was examined without making an explicit source correction. One conclusion was that the attenuation effect is about the same for GBA and WRA, which seems consistent with the data in Figure 9. Another was that the effective t* in the 0.5-3.0 Hz band is somewhat less for EKA and somewhat more for YKA. There is some suggestion of these differences in the source-corrected spectra in Figure 9, but the differences do not appear large enough to be significant. The one truly exceptional feature in Figure 9 is the character of the NORSAR spectrum above 4 Hz. However, at lower frequencies the NORSAR spectrum is about the same as the others.

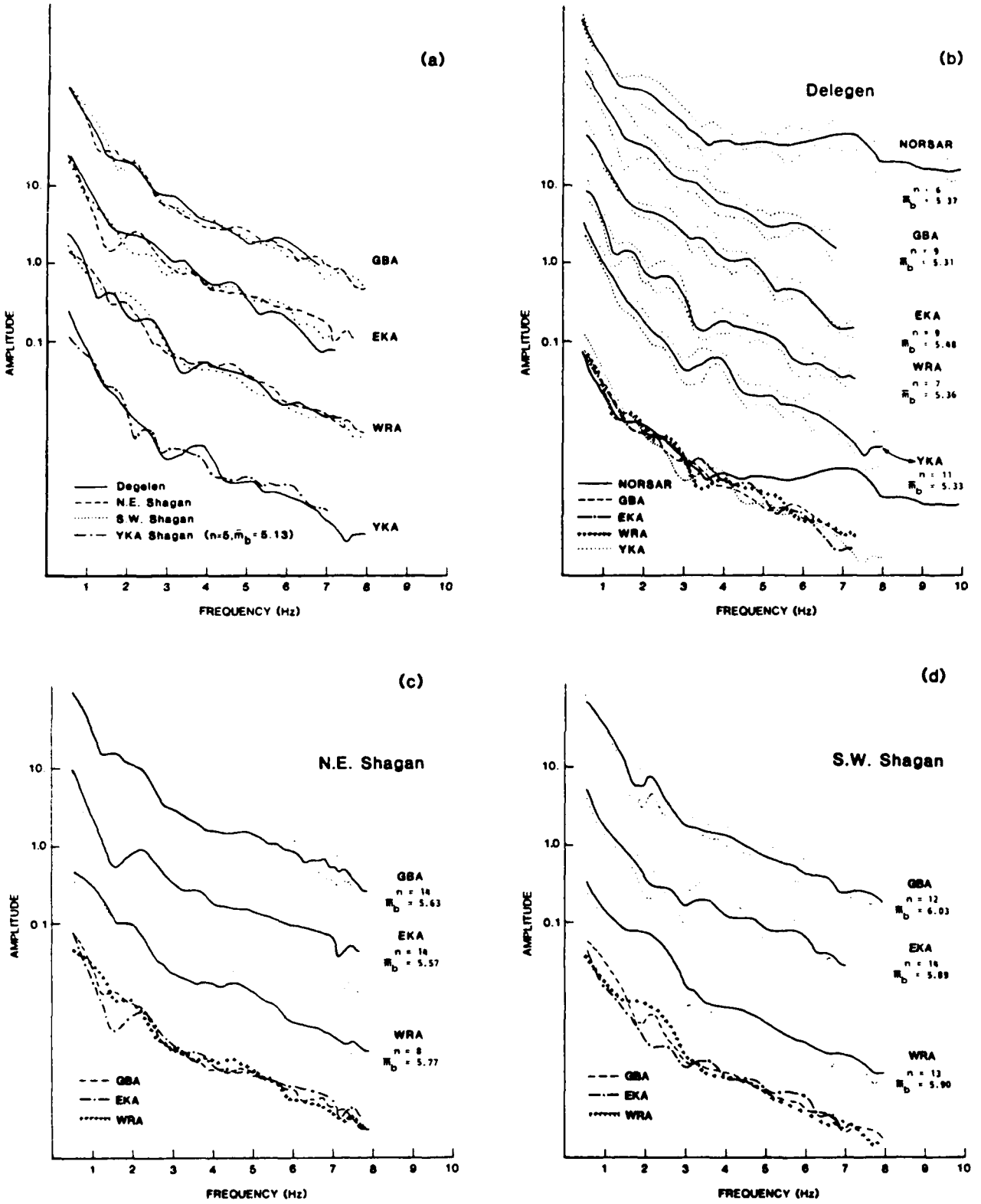

Figure 9 Source corrected path spectra are plotted for each data set considered. In (a) we compare the path spectra from different portions of the test site at each UKAEA station (at YKA there are too few data to bisect the Shagan River site). In (b-d) the mean spectrum for each path is shown with dotted line indicating the sample standard deviation. At the bottom of each of these is shown a comparison of the mean spectra for the paths from that particular source area to each station.

Attenuation Models

The spectra in Figure 9 can be fit with two effective attenuation models, one for the E. Kazakh-NORSAR path, and one for the paths to the UKAEA stations. An attenuation model for the latter was determined in Paper I and is based on the absorption band model of Minster (1978). To match the constant slope decay above 2.5 Hz, it was necessary to add a second Q distribution which dominates the attenuation at high frequency. This two-part model is formulated in terms of three parameters (t_0^*, τ_m, and t_1^*). The t_0^* and τ_m specify the absorption band, with t_0^* the ratio of travel time (T) to Q at long periods. The $\tau_m = (2\pi f_m)^{-1}$, where f_m is the frequency where $T/Q = 0.5\ t_0^*$. The t_1^* is the T/Q for the second portion of the attenuation model. There are strong tradeoffs, and the data are not adequate to resolve these three parameters with much precision. However, an advantage of this two-part model is that it appears to represent an important distinction between attenuation mechanisms. That is, the absorption band seems to represent attenuation by energy absorption, while the t_1^* appears to represent attenuation mainly due to scattering (Paper I).

In Figure 10 we show effective attenuation models for these paths. For the UKAEA paths we use the preferred model of Paper I. For the NORSAR path the spectral flattening at high frequency results from eliminating the t_1^* from the model. When $Q \propto f$, as it is at high frequency in the absorption band model, the effect of attenuation is to multiply the spectrum by a constant. While t_1^* is absent from the NORSAR model, scattering attenuation can still be contributing to the attenuation at high frequency if it is represented by $Q \propto f$. Indeed, models for single scattering by distributed random inhomogenieties indicate that Q has this form at sufficiently high frequency (e.g., Sato, 1984).

In Figure 11 we plot the spectral effect of the attenuation models with the source-corrected path spectra for Degelen explosions recorded at NORSAR and GBA. Also plotted are spectra for synthetic seismograms

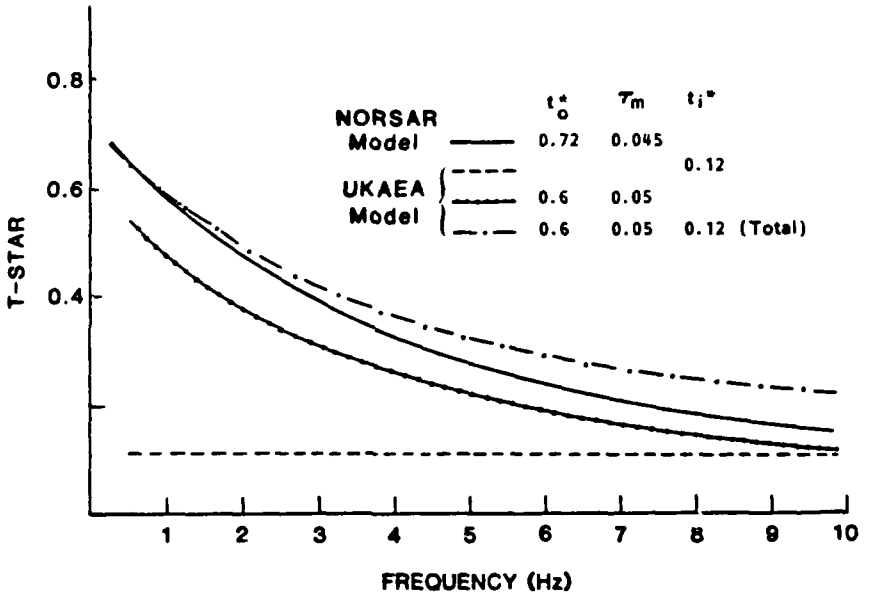

Figure 10 The effective attenuation models for two paths are shown in terms of t* versus frequency. The NORSAR path is represented by a single absorption band. The model for the UKAEA paths includes two parts and each is plotted, as well as the total t* for these paths.

which have been processed with the same time window and source corrected. The synthetics were computed with simple plane-layered structures at the source and receiver, so the spectrum is shaped almost entirely by the attenuation model and P-pP interference. The P-pP lag time chosen is consistent with a depth of 600 meters in a granite with an average overburden velocity of 5 km/sec. Generally the peaks and nulls indicative of pP interference are not clearly seen in explosion P wave spectra. In fact, they are even suppressed in theoretical seismograms when the source is obtained from numerical simulations that include near-source nonlinear behavior (e.g., Bache, 1982). The NORSAR Degelen spectrum may be unusual in this respect since it seems likely that the trough and peak near 3.5 and 7 Hz are associated with P-pP interference. Note that the same feature is not seen consistently in the UKAEA Degelen spectra (Figure 9b).

Figure 11 shows that the selected attenuation models fit the data rather well, especially when we consider that the synthetic spectra exaggerate the influence of pP inteference and omit all other features (e.g., source and receiver region reverberations) that modulate the spectrum. The two attenuation models were selected to be as nearly similar as possible. Variations of t_0^* by 0.1 seconds (or more on the high side) are easily accomodated by changing τ_m by amounts on the order of 0.01. Some of these tradeoffs are illustrated in Paper I.

Spectra for Long Windows

In Paper I spectra for the short (typically 2.5 seconds) time windows were compared to spectra computed the same way but with 10 second windows starting just before the P onset. In most cases long window spectra have more high frequency energy above 2.5 Hz, indicating that the coda is much richer in high frequencies than the initial P wave. This is evidence that scattering attenuation is important at high frequency.

A similar comparison of short and long time window NORSAR Degelen

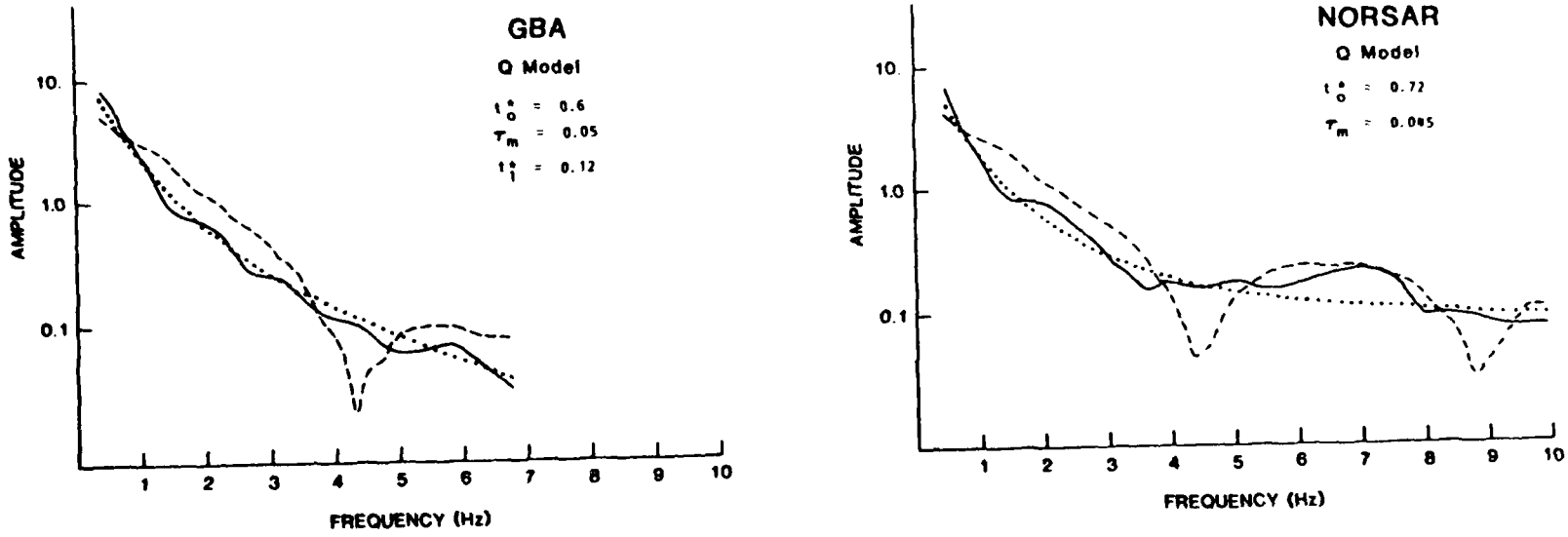

Figure 11 Source-corrected spectra for the paths from Degelen to GBA and NORSAR are plotted with the effect of the Q model specified. Also shown is the spectrum of a synthetic seismogram (processed the same way as the data) for this Q model and a P-pP lag time of 0.22 seconds.

spectra is made in Figure 12. The only important difference between the two is that the broad null between 3 and 6 Hz is much less prominant in the long window spectrum. This supports the earlier conjecture that this trough is associated with pP interference, since a longer window would be expected to reduce the influence of this interference.

Discussion

Stacking the recordings from the array elements and then from similar sources (in this case underground nuclear explosions), we are able to compute smooth spectra shaped almost entirely by the path attenuation and the source spectrum. The key feature of the source spectrum is its corner frequency, which varies with yield (or m_b) and depth of burial. It can also vary with the properties of the local geology, but we assume these variations are not important within the eastern Kazakhstan test site. We corrected these data with the Mueller and Murphy (1971) granite source. This appears to account for spectral differences that correlate with m_b. Also, the apparent attenuation effects are nearly the same for explosions occurring in different portions of the test site.

The source-corrected spectra are shown in Figure 9 and are all nearly the same below 3 Hz. Above 3 Hz the NORSAR spectrum is the one exception and has much more high frequency energy. This feature is independent of the assumptions about the source spectrum. Also, the signal and noise spectra shown in Figures 3-6 all show this feature and include no indication of any instrumentation or processing errors.

The similarity of the attenuation effects at low frequency for all five paths is a robust feature of the data. However, the precise nature of this effect is dependent on assumptions about the source spectra. For example, if we assumed the corner frequency was uniformly (by some small fraction) higher for every event, we would get source-corrected spectra that are just as consistent, but more steeply sloping at low frequency. The models are constrained by the requirement for con-

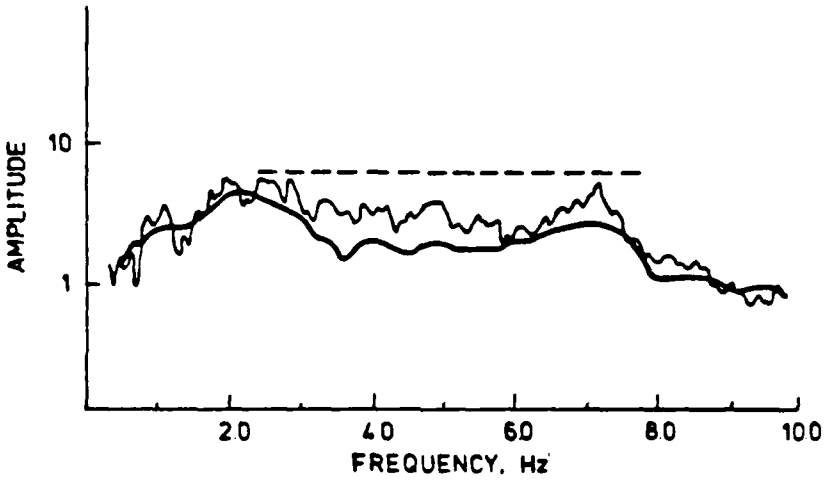

Figure 12 The path average spectrum obtained by stacking the event spectra in Figure 4 (based on individual element spectra computed with 2.2-2.3 second time windows) is compared to a path average spectrum computed the same way from element spectra computed with 10 second windows.

sistency among events at different m_b and in different areas. We have not fully explored the tradeoffs, but uniform changes in corner frequency of up to 50% are difficult to rule out, based on spectral consistency alone.

The path attenuation effects fall into two classes, and these are fit with attenuation models in Figure 11. The main difference between the two is that the t_1^* is omitted for the NORSAR path model. This allows Q to become nearly proportional to frequency at high frequency. Since physical mechanisms for absorption must have $Q \propto f$ above some high frequency limit on the relaxation spectrum, absorption band models anticipate behavior of this type (e.g., Anderson and Given, 1982). These NORSAR spectra show that such behavior does indeed exist. For most paths it is difficult to observe, perhaps because it is usually masked by scattering attenuation. This seems to be the case for the paths to the UKAEA stations.

Frequency dependence of Q is important in the 0.5-3.0 Hz band. It can be represented by an absorption band with long period t_0^* of 0.6-0.7 seconds and a τ_m near 0.05 seconds. There are tradeoffs between the t_0^* and τ_m and between the attenuation model and the assumptions about the characteristic source function, but these estimates seem most consistent with results from other studies of explosion source theory and attenuation.

We have no explanation for why the high frequency attenuation is so different for the NORSAR path, but it appears to be associated with difference in the contribution of scattering attenuation. The comparison of long and short window spectra in Paper I and Figure 12 support this hypothesis. We note that the NORSAR spectrum does show the effect of some additional attenuation above 7 Hz as is seen clearly in the one example where the spectrum could be computed to 20 Hz. A better understanding of attenuation mechanisms and their spectral effect at high frequency is needed to understand why this occurs.

As an important sidelight of this investigation, we note that the maximum signal/noise occurs at frequencies greater than 5 Hz for these NORSAR recordings of teleseismic P waves. When Q is nearly proportional to frequency, the P wave spectrum is nearly proportional to f^{-2}, the spectral decay of the source function. At NORSAR the noise spectrum often decays as f^{-2}, and on quiet days it decays as $f^{-2.5}$ to frequencies beyond 10 Hz (Bungum et al., 1985). Thus, the signal/noise will not decrease until some additional attenuation effect begins to degrade the P wave spectrum and/or the noise spectrum flattens to less than f^{-2} decay. The computed spectra indicate that some additional attenuation effect does become important above 7 Hz. Also, we see that increasing noise often degrades the signal/noise above 7 Hz. Thus, it appears that the maximum signal/noise occurs at 7-8 Hz for P waves on this path. If this is typical of Eurasian paths, this observation suggests that P wave detection capability would be enhanced by more emphasis on data at these high frequencies.

Acknowledgements

Much of this work was done while one of the authors (TCB) was a Visiting Research Fellow at MOD(PE), Blacknest, Brimpton, England. This visit was supported by the United Kingdom Ministry of Defense and by the United States Defense Advanced Research Projects Agency under Contract DNA-001-83-C-0838, which was administered by the Defense Nuclear Agency. John Young and Lolitia Bache were responsible for much of the data processing at Blacknest. Discussions with Peter Marshall, Blacknest, also played an important part in developing the ideas presented here. At NORSAR, Svein Mykkeltveit made valuable contributions in data preparation and analysis and in discussing the results. Paul W. Larsen did the work with the PDR-2 recordings and helped verify the quality of the NORSAR data. Portions of this research were supported by the Defense Advanced Research Projects Agency under Contract F08606-84-C-0002 (monitored by the Air Force Technical Applications Center) and Contract F19628-85-C-0021 (monitored by the Air Force Geophysics Laboratory).

References

Anderson, D.L. and Given, J.W., 1982. Absorption band Q model for the earth, J. geophys. Res., 87, 3893-3904.

Archambeau, C.B., Flinn, E.A. and Lambert, D.G., 1969. Fine structure of the upper mantle, J. geophys. Res, 71, 5825-5865.

Bache, T.C., 1982. Estimating the yield of underground nuclear explosions, Bull. seism. Soc. Am., 72, 5131-5168.

Bache, T.C., Marshall, P.D., and Bache, L.B., 1984. Q for teleseismic P waves from Central Asia, J. geophys. Res., 90, 3575-3587.

Bungum, H., Mykkeltveit, S., and Kvaerna, T., 1985. Seismic noise in FennoScandia, with emphasis on high frequencies, (in preparation).

Chang, A.C. and von Seggern, D.H., 1980. A study of amplitude anomaly and m_b bias at LASA subarrays, J. geophys. Res., 85, 4811-4828.

Der, Z.A., McElfresh, T.W. and O'Donnell, A., 1982. An investigation of the regional variations and frequency dependence of anelastic attenuation in the mantle under the United States in the 0.5-0.4 Hz band, Geophys. J. R. astr. Soc., 69, 67-99.

Der, Z., McElfresh, T., Wagner, R. and Burnetti, J., 1985. Spectral characteristics of P waves from nuclear explosions and yield estimation, Bull. seism. Soc. Am., 75, 379-390.

Haskele, N.A., 1967. Analytic approximation for the elastic radiation from a contained underground explosion, J. geophys. Res., 2583-2587.

Helmberger, D.V. and Hadley, D.M. 1981. Seismic source functions and attenuation from local and teleseismic observations of the NTS events Jorum and Handley, Bull. seism. Soc. Am., 71, 51-67.

Marshall, P.D., Lilwall, R.C. and Bache, T.C., 1984. Body wave magnitudes and locations of Soviet underground explosions at the Semipalatinsk Test Site, A.W.R.E. Report No. O-16/84, HMSO, London.

Minster, J.B., 1978. Transient and impulse responses of a one-dimensional linearly attenuating medium - II. A parametric study, Geophys. J.R. astr. Soc., 52, 503-524.

Mueller, R.A. and Murphy, J.R., 1971. Seismic characteristics of underground nuclear detonations, Bull. seism. Soc. Am., 61, 1675-1692.

Murphy, J.R. 1977. Seismic source functions and magnitude determinations for underground nuclear detonations, Bull. seism. Soc. Am., 67, 135-158.

Mykkeltveit, S., Astebol, K., Doornbos, D.J. and Husebye, E.S., 1983. Seismic array configuration optimization, Bull. seism. Soc. Am., 73, 173-186.

Ringdal, F. and Husebye, E.S., 1982. Application of arrays in the detection, location and identification of seismic events, Bull. seism. Soc. Am., 72, 5201-5224.

Sato, H., 1984. Attenuation and envelope formation of three-component seismograms of small local earthquakes in randomly inhomogeneous lithosphere, J. geophys. Res., 89, 1221-1241.

SECTION III

AN INVESTIGATION OF THE DEGRADATION OF TELESEISMIC DETECTION CAPABILITY CAUSED BY LARGE EARTHQUAKES

Steven R. Bratt and Thomas C. Bache
Science Applications International Corporation
San Diego, CA

6 September 1985

Introduction

Our objective is to determine the extent to which the detection capability of a worldwide monitoring network is degraded during the period immediately after a large earthquake. The motivation is provided by the need to assess the seismological capability to monitor treaties banning or limiting underground nuclear explosion testing. Estimates of the detection threshold of the monitoring network play a crucial role in that assessment. We expect the detection threshold of a network to increase for a time after a large earthquake, and this raises the possibility that a determined (and patient) state could conduct a clandestine nuclear test by hiding its seismic signature in the signal of the larger earthquake. This is called the "Hide-in-Earthquake" (HIE) evasion scheme and has been discussed in many previous studies and reviews of nuclear test monitoring capability (e.g., Filson, 1973; Blandford, 1977; Evernden, 1976a,b).

While the HIE evasion scheme is a recognized problem for nuclear test monitoring, we are not aware of any empirical study that demonstrates the actual effect of large events on the capability to detect small ones. The main reason is that it is difficult to design an experiment to estimate how many events are <u>not</u> detected by a network. One way to circumvent this problem is to study a large data base and compare the seismicity after large earthquakes to the average seismicity level. With enough data, deviations from the average will provide a measure of undetected events. This is the experiment we have chosen to conduct.

Data

The International Seismic Centre (ISC) Bulletin cataloging worldwide seismicity provides a large data base. However, this bulletin is poorly suited for examination of changes in the seismicity level because of temporal variations in the network configuration and

inconsistencies and bias in the magnitude data. For example, Burnetti and Rivers (1984) analyzed the ISC Bulletin, but found that the scatter in the ISC data was too large to permit meaningful conclusions about HIE effects.

Our study uses a bulletin derived by Ringdal (1984) which is designed to reduce the many of the inconsistencies that affect the ISC Bulletin. Ringdal's bulletin was constructed by reprocessing 10 years of data (1971-1980) reported to ISC by 115 stations selected for their global distribution, consistency, and high quality reporting. The bulletin includes all earthquakes which were reported by at least four stations, with at least one at a range between 21 and 100 degrees. A total of 74109 events meet these criteria, including nearly all earthquakes for which any teleseismic reports are listed in the ISC bulletins.

The m_b in the ISC bulletins are computed by averaging the m_b from all stations reporting P amplitudes. However, such magnitudes can be significantly biased because of network truncation. Since stations typified by low amplitude signals are less likely to detect signals, an arithmetic mean will tend to be biased toward higher m_b. This bias in the m_b of small events will then lead to bias in the estimated detection threshold for the network. The maximum likelihood technique (Ringdal, 1976) is designed to minimize this bias by including bounds on the P wave amplitudes at non-detecting stations derived from empirical estimates for the detection threshold at each station. Ringdal (1984) computed the maximum likelihood m_b for each event in his bulletin, and it is these magnitude data that we examine in this study.

The maximum likelihood m_b are about the same as the ISC m_b for $m_b > 5.2$. At lower magnitudes, the ISC m_b are biased high, with the typical difference becoming as large as 0.4-0.5 when the maximum likelihood m_b is 4.0-4.5. Ringdal (1984) also estimated the global teleseismic

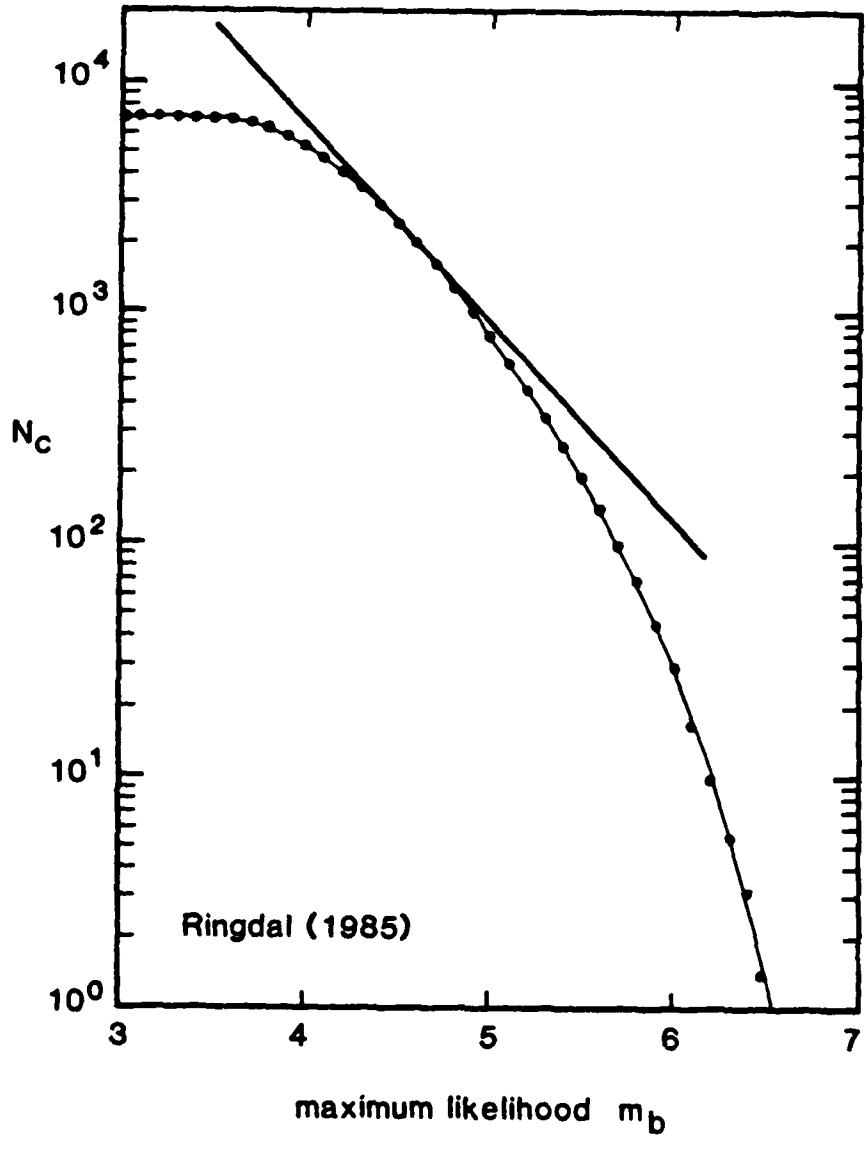

Figure 1 Cumulative recurrence statistics (using maximum likelihood m_b) are plotted for the bulletin of Ringdal (1984). The straight line representing Equation (1) is also plotted.

detection threshold of his network. Requiring a 90% probability of detection by at least four stations, the incremental thresholds vary from 3.9-4.4 (maximum likelihood m_b) in the northern hemisphere to 4.3-4.7 in the southern hemisphere. Globally, the threshold is 4.45.

Cumulative statistics for events in Ringdal's bulletin are shown in Figure 1. A fit to these data (constrained to have a 0.90 slope) is:

$$\log N_c = 7.44 - 0.90 m_b, \qquad (1)$$

where m_b is the maximum likelihood magnitude and N_c is the cumulative number of events with magnitude $\geq m_b$.

Experiment

We investigate the effect of large earthquakes on the detection threshold of Ringdal's (1984) network by comparing the number of events reported after large events to the number expected, based on the seismicity averaged over the ten years of the bulletin. The latter is represented by the expected number of events per unit time, or recurrence frequency, F_e. Assuming a constant level of seismicity and excluding periods after large events, this is given by:

$$F_e = \frac{N(m) - n(m,M,t)}{T-kt}, \qquad (2)$$

where T is the total time (ten years) and k is the number of earthquakes with maximum likelihood $m_b \geq M$ during that time. The N(m) is the total number of earthquakes in an increment about magnitude m, and n(m,M,t) is the number of events in the same magnitude increment within time t after all earthquakes exceeding magnitude M. For the cases of interest, n and kt are relatively small. Then F_e is not much different from N/T, which is the average number of earthquakes per unit time in the entire bulletin.

The recurrence frequency, F_d, for events actually detected following large earthquakes is given by:

$$F_d = \frac{n(m,M,t) - a(m,M,t,r)}{kt} \qquad (3)$$

This includes a correction for aftershocks, a(m,M,t,r), which is the number of events occurring within time t and radius r of the n(m,M,t) large earthquakes. Exclusion of aftershocks from F_d permits us to isolate the effects of great earthquakes on the detection of events occurring elsewhere in the world.

It is clear from (3) that F_d is sensitive to a(m,M,t,r), and therefore to the choice of r. Ambiguity in the physical definition for what constitutes an aftershock and location inaccuracies make it difficult to do this on a physical basis. Instead, we empirically determined an r that appears to encompass most aftershocks. This was done by calculating a(m,M,t,r) for several values of t and r. We then approximated the number of aftershocks per unit length along the fault by the relation:

$$\rho_a = \frac{a(m,M,t,r)}{2\ r}, \qquad (4)$$

where ρ_a is the number of additional aftershocks added to the total by increasing the radius of the presumed aftershock circle by Δr. Thus, ρ_a should approach some small constant number as r increases beyond the radius that encompasses most aftershocks. Figure 2 shows ρ_a for M = 6.2 and t = 0.5 and 5.0 hr. It is plotted for discrete values of r from 50 to 750 km. The figure shows that ρ_a becomes nearly constant for r >200 km. Therefore, the vast majority of the aftershocks are located within this radius. Based on Figure 2, we assume r to be 200 km in most of the calculations, but we will also show how F_d changes when r = 100 km.

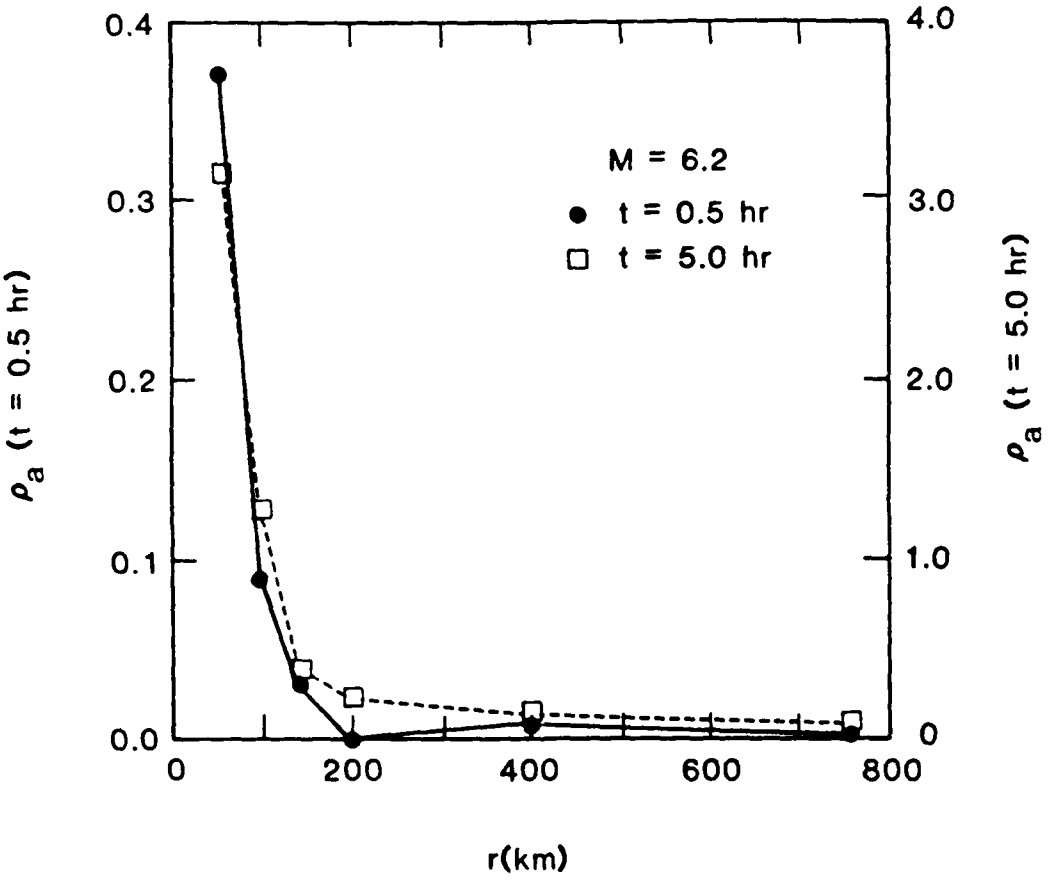

Figure 2 The plots show ρ_a, which is the number of aftershocks per unit length along the fault, as a function of distance r from the main event. The ρ_a is plotted for M = 6.2 and two values of t.

A useful method of comparing the detected (F_d) and expected (F_e) recurrence frequencies is through a ratio of the two quantities:

$$R = \frac{F_d}{F_e} \quad . \qquad (5)$$

We consider R both in an incremental sense, in which F_d and F_e are as previously described, and in a cumulative sense, where N(m), n(m,M,t), and a(m,M,t,r) are replaced by the total number of events less than magnitude m. In either case, R represents the fraction of the expected number of events of (or less than) magnitude m actually detected by the network following earthquakes larger than magnitude M.

Before examining the results, consider some of the advantages and limitations of this procedure. First, the 10 years of earthquake data provide a large sample, and therefore a good estimate for the expected recurrence frequency, F_e. Also, equation (3) provides a ten year average of F_d. However, though the largest effects on the network threshold are expected after the largest earthquakes, there are relatively few of these earthquakes. Thus, there is a trade-off in selecting the magnitude M, with larger values preferred to determine the maximum effect on the network threshold, and smaller values preferred to obtain large samples and more reliable statistics.

We also note that even when events are detected after large earthquakes, we might expect some magnitude bias due to network truncation, since stations where the signals are unusually large are more likely to report the signals from the smaller events. Ringdal's maximum likelihood m_b calculations are based on average station detection thresholds, and so do not account for the increased "noise" levels caused by the large earthquakes.

Results

We have calculated recurrence frequencies, F_d, F_e, and their ratio R for three values of M (6.2, 6.0, 5.8) and for three time intervals (t = 0.5, 1.0, 5.0 hr) following the events with $m_b \geq M$. The event statistics used for these calculations are summarized in Table 1. The F_e and F_d were calculated for 0.1 increments of m, then smoothed with a three-point moving average. They were also normalized to 1000 hours (F_e and F_d are multiplied by 1000/kt), so recurrence frequencies for different M and t can be conveniently compared.

Figure 3 shows F_d and F_e, and there are a number of interesting features in this figure and Table 1. For example, there are 96 events in the bulletin with $m_b \geq 6.2$, so 0.55% of the total duration (T = 10 years) of the bulletin falls within 5 hr of these earthquakes. We removed from consideration 507 "aftershocks" that occurred within 5 hr and 200 km of these 96 earthquakes. These earthquakes represent 0.68% of the total number of events recorded during the 10 year period. Thus, the seismicity level due to aftershocks alone is slightly above average worldwide levels.

The curves shown in Figure 3 exhibit consistent trends for all three M, even though the statistical sample varies from quite small (there are only 26 events within one-half hour of $m_b \geq 6.2$ earthquakes) to rather large (there are 2704 earthquakes, or 3.7% of the total in the bulletin, within 5 hours of $m_b \geq 5.8$ earthquakes). For t = 0.5 hr, F_d is less than F_e for all values of m. Also, the differences between F_d and F_e diminish as t increases.

An initially surprising aspect of these curves (which complicates the interpretation) is that F_d is less than F_e for $m_b > 4.7$ in most cases. There is no plausible physical reason why this should be a real feature of earthquake recurrence statistics. In fact, we would expect F_d to approach F_e in this magnitude range. One possible cause of the apparently low value of F_d is the choice of aftershock radius r. As is evident from equation (3), if r is too large, a(m,M,t,r) will also be

TABLE 1

Event Statistics for Three Time Intervals and Three M

M	Total k*	Time Interval (t)	Total Time (kt)	Events**	Aftershocks a(m,M,t)
6.2	96				
		0.5 hr	48 hr	23	49
		1.0	96	56	117
		5.0	480	346	507
6.0	290				
		0.5 hr	145 hr	76	122
		1.0	290	183	272
		5.0	1450	1091	1080
5.8	694				
		0.5 hr	347 hr	185	219
		1.0	694	462	470
		5.0	3470	2565	1558

*Total number of events with $m_b \geq M$ in the ten-year bulletin

**In the notation of Equations (2) and (3), this is n(m,M,t) - a(m,M,t)

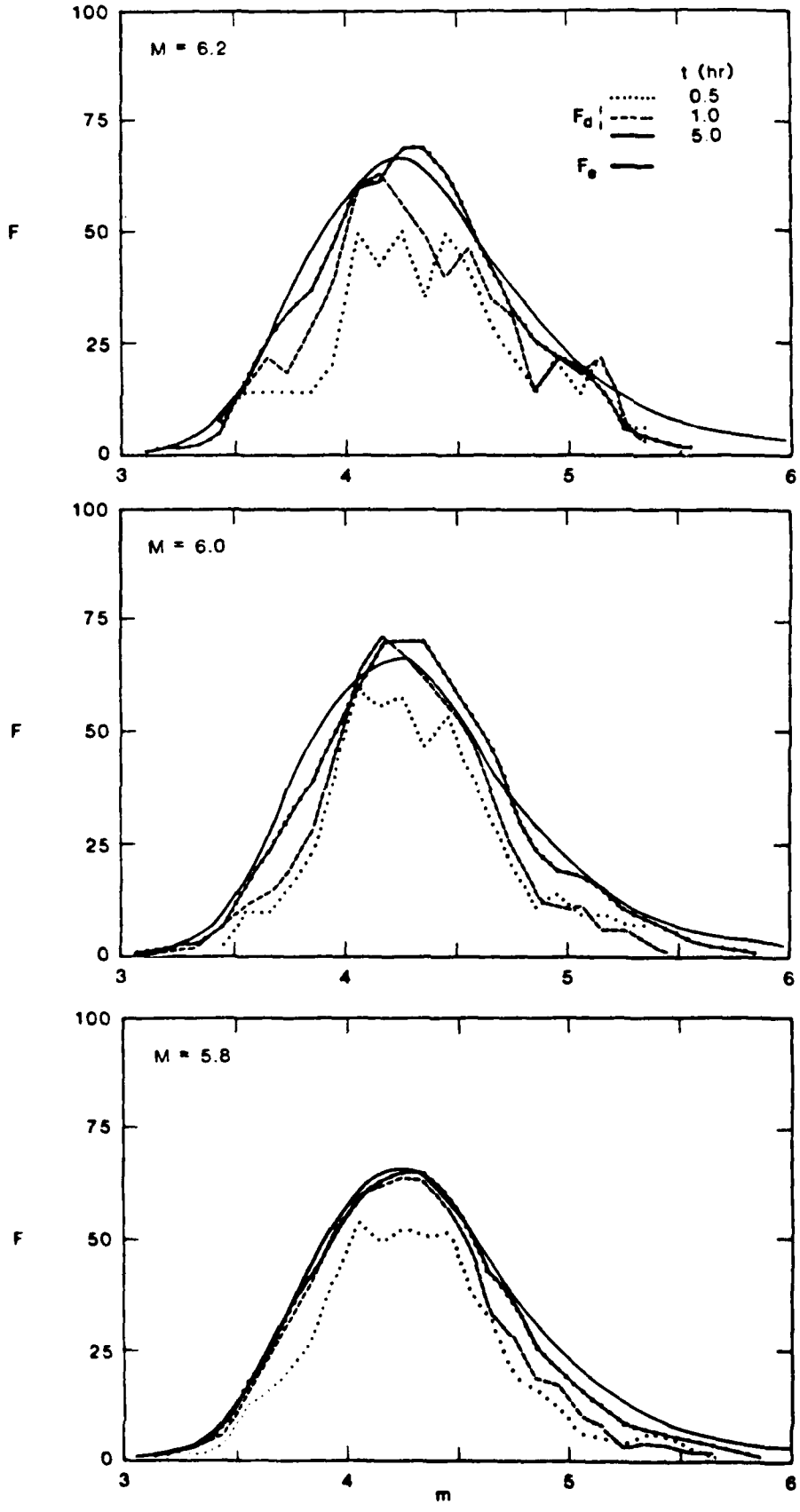

Figure 3

The incremental number of events expected (F_e) and detected (F_d) per 1000 hr is plotted for three M and three t. The assumed aftershock radius r is 200 km.

too large. F_d will then underestimate the true number of independent earthquakes. To test this hypothesis, we computed F_d using several smaller values of r. Figure 4, for example, shows F_d compared to F_e for M = 6.2 and r = 100 km. With this smaller r, F_d is nearly equal to F_e for $m_b > 4.7$. There is also a region between m_b 4 and 5 where F_d is much larger than F_e. This is almost certainly due to r being too small, and F_d being biased by including aftershocks. This is just what should be expected from the results in Figure 2. Thus, the r = 200 km data (Figure 3) give more reliable results.

The only features of the data in Figure 3 that are difficult to explain are $F_d < F_e$ for $m_b > 4.7$, and $F_d > F_e$ in the mid-magnitude range for some cases. The most likely cause is that the earthquakes in F_d have biased m_b. That is, it seems likely that the m_b for the small earthquakes in F_d are biased high, and the m_b for the larger earthquakes contributing to F_d are biased low. The result is a concentration of F_d in the mid-magnitude range. Note that the maximum likelihood m_b used in this study were calculated with estimates for the average station detection thresholds. However, the coda of large earthquakes will substantially raise the station detection thresholds. This will truncate the sample by deleting stations with weaker signals, thus causing the maximum likelihood m_b to be biased high for small events detected in the coda of much larger ones (Ringdal 1978, pointed out this problem). An analogous effect at high m_b is probably the cause for $F_d < F_e$ for $m_b > 4.7$. We note that Ringdal (1984) made no attempt to correct for the bias introduced by network truncation caused by clipping of strong signals (von Seggern and Rivers, 1978) at some stations. Great events are more likely to be clipped at stations typified by large signals, so these stations will not provide amplitude data. The effect is bias, or m_b saturation, and is clearly seen in the cumulative recurrence curve of Figure 1. There will be a period of time where nothing can be measured on the records at these stations, so no amplitude data will be reported for smaller earthquakes either. Thus, we expect the average magnitude from those stations that do report amplitude data to be biased downward. While this bias in F_d makes interpretation more difficult, some estimates can be made. This

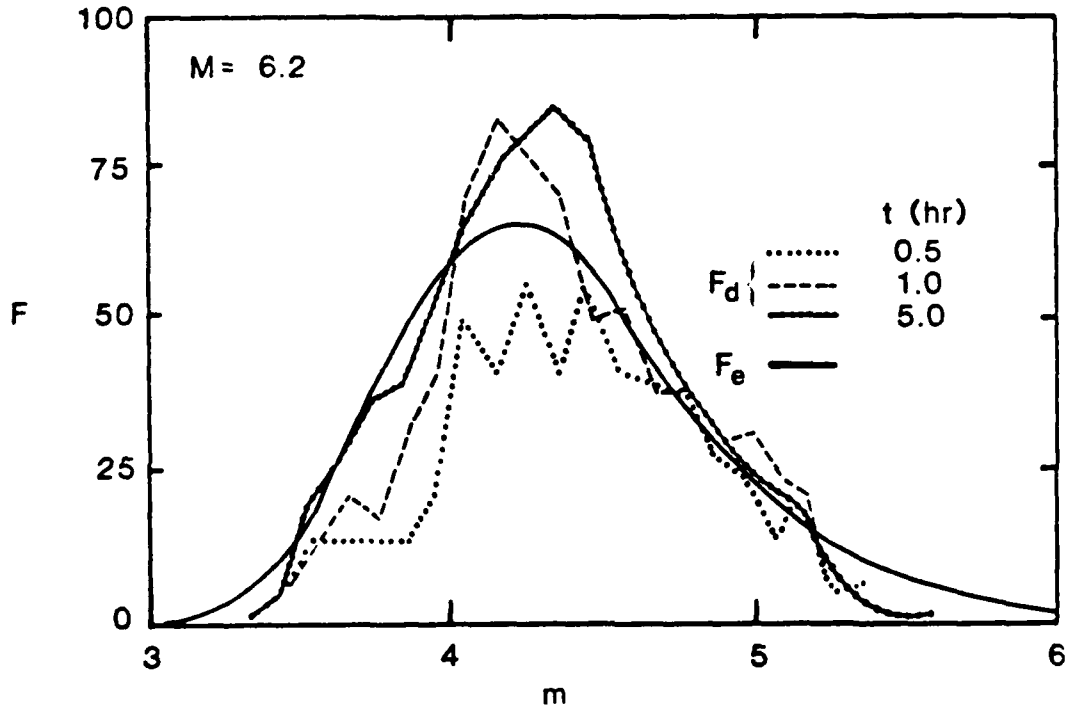

Figure 4 The incremental number of events expected (F_e) and detected (F_d) per 1000 hr is plotted for M = 6.2. The assumed aftershock radius r is 100 km.

is because the bias changes the shape of the F_d curves, but should not have much effect on the total area beneath them. For t = 0.5 and 1.0 hr in Figure 3, the area under F_d is substantially less than the area under F_e, so some events are clearly being missed by the network. The same effect can also be seen by studying the ratio R (equation 5). This ratio indicates the number of events actually detected, compared to the number that would have been detected by this network (assuming uniform seismicity), if the earthquakes with $m_b \geq M$ had not occurred. In Figures 5 and 6, R is plotted in terms of incremental and cumulative statistics, respectively. These plots extend only to m_b 4.5, which is just above the peak in the curves in Figure 3.

Several robust trends are seen in the cumulative ratios of Figure 6. Comparing the plots for different M, it is clear that the larger M are associated with smaller R; that is, larger earthquakes tend to cause relatively fewer events to be detected. The ratio is smallest in the first 0.5 hr after large earthquakes, and increases with the length of time (t) considered. Also, the ratio increases with m; that is, relatively more small events are hidden than large ones. These are all features we expect to see, and their consistency lends credibility to the results.

We can estimate the fraction of hidden events smaller than some magnitude m by computing the ratio (R_c) of the cumulative recurrence frequencies at m. The reliability of this estimate depends on the value of m. If we chose the upper bound (m_u) for the presence of upward bias in the m_b of the events in F_d, then R_c at m_u will be an unbiased estimate for the proportion of undetected events. It is difficult to estimate m_u with any precision, but it is likely to be between m_b 4.0 and 4.5, since this is the range where F_d sometimes exceeds F_e. If the bulge in the F_d curve were mainly due to downward

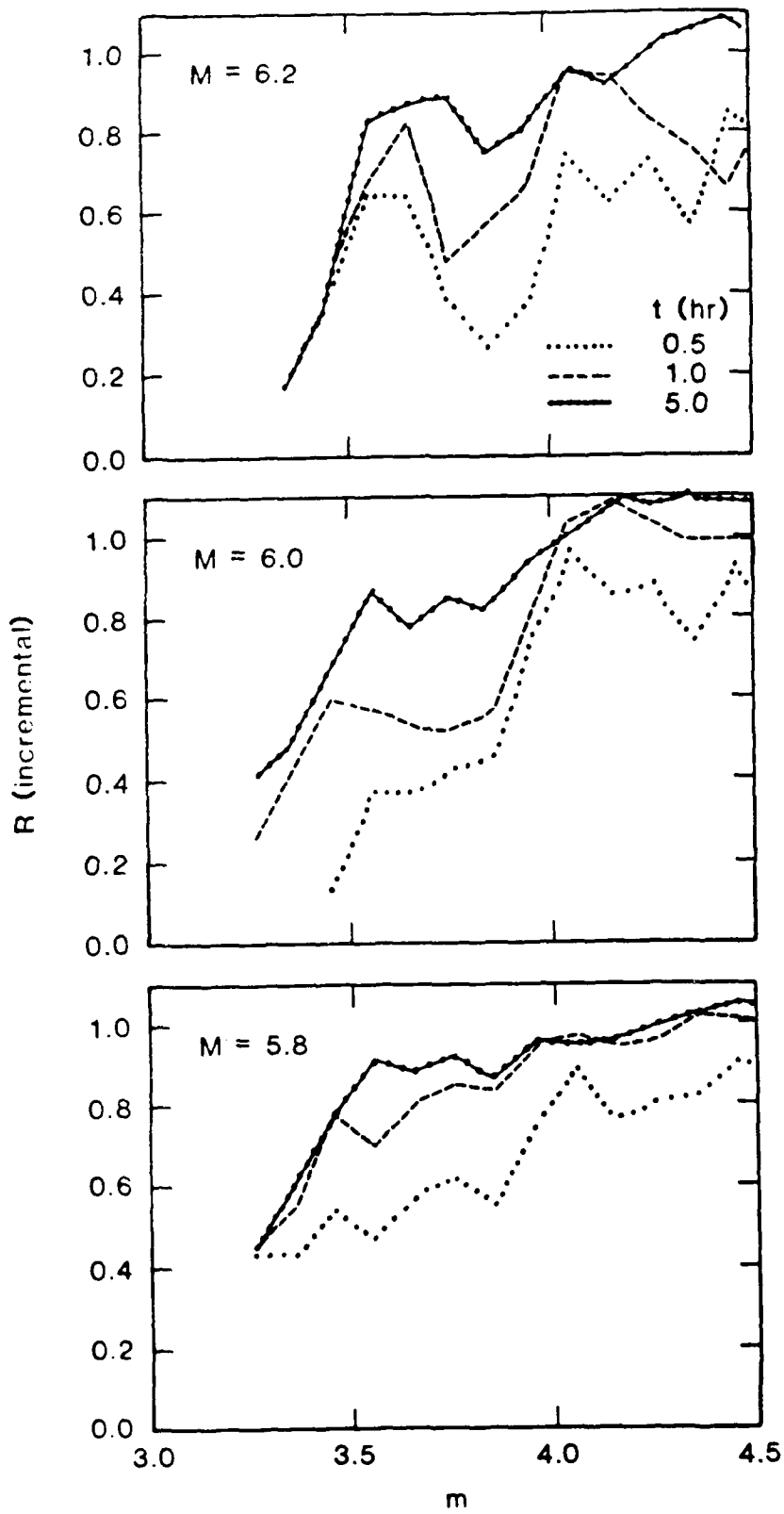

Figure 5 The incremental ratio (R) of detected (F_d) to expected (F_e) recurrence frequencies is plotted for three M. Both F_d and F_e were computed incrementally before computation of R.

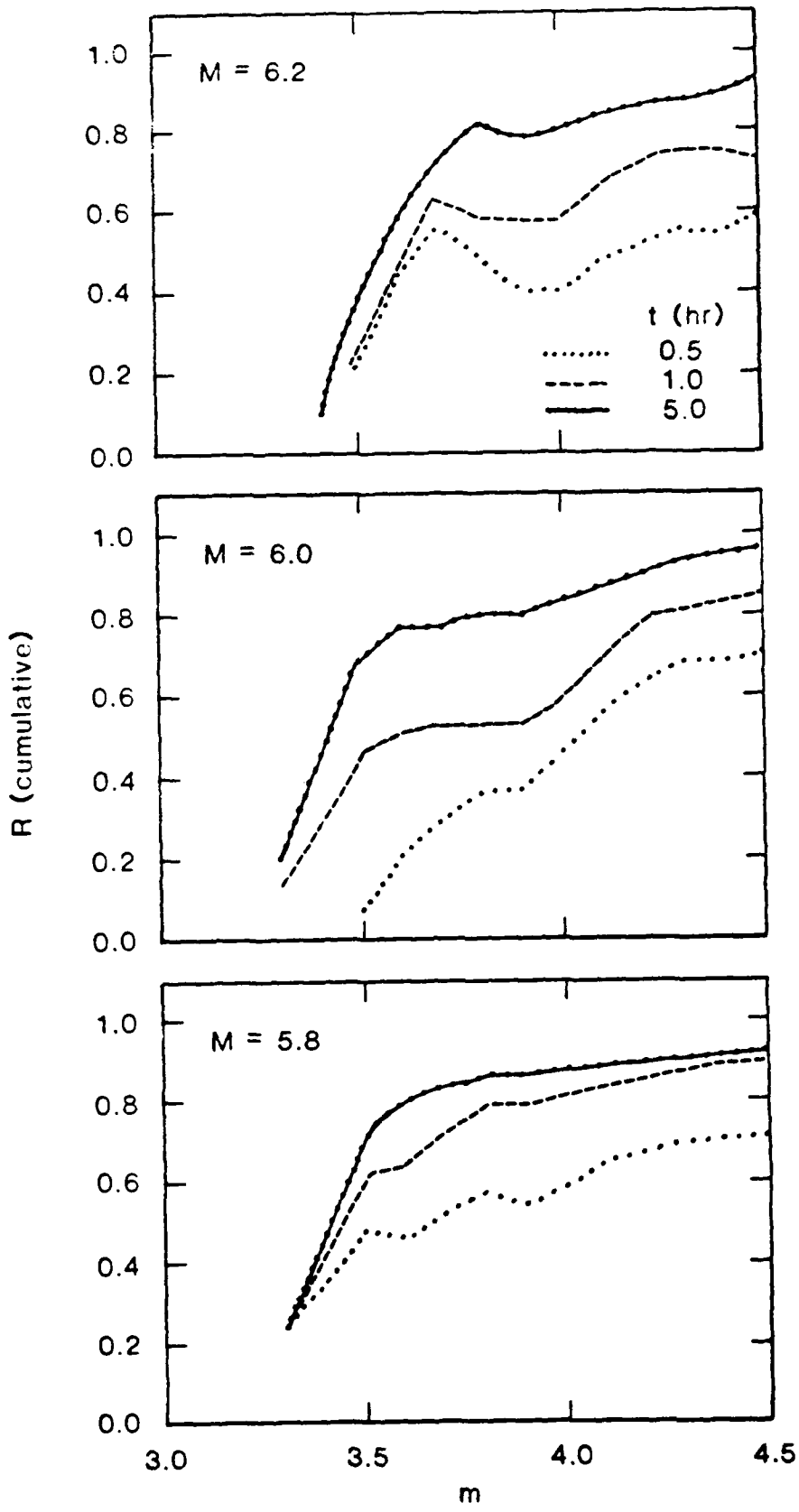

Figure 6 The cumulative ratio (R) is plotted for three M. Both F_d and F_e are computed cumulatively, so each is then the number of events with $m_b < m$ per unit time. The R is their ratio.

bias in the m_b for larger events, then m_u would be close to 4.0. If it is mainly due to upward bias in the m_b for smaller events, then m_u would be close to 4.5. The symmetry in the curves in Figure 3 suggests that m_u is somewhere between the two extremes.

The fraction of events that fail to be detected ($1-R_c$) can be estimated directly from the cumulative ratio curves in Figure 6 for any estimate of m_u. The fraction of missed events is given in Table 2 for each case considered and also for two choices of m_u, 4.0 and 4.5. There are two values for each case. One is the fraction, which can be read as a percentage. For example, about 36% of events with $m_b < 4.5$ that would normally be detected by this network are missed in the half-hour periods following $m_b \geq 6.2$ events. The other value given in the table is an estimate for the number of events missed. For example, over these ten years there were 48 hours following $m_b \geq 6.2$ events. During this time 25 events were expected, and 16 were detected. Hence, we estimate that 9 events were missed.

The two values in Table 2 have different significance. The fraction is an indication of how the network detection threshold changes. High fractions (> 0.2) occur for larger events or shorter time intervals. On the other hand, the number missed is mostly controlled by the length of the time period considered. Thus, even a small increase in the network detection threshold (i.e., fraction < 0.2) can cause a large number of events to be missed if the time period is long so a large number is expected. The fraction is a much more significant quantity for the HIE evasion scenario.

The fraction of events apparently hidden by the large earthquakes indicates the effect of these earthquakes on the network detection capability, though it is difficult to quantify. It seems clear that the detection capability of the network is significantly affected for periods up to at least one hour following events with $m_b \geq 6.0$ and at least 30 minutes following events with $m_b \geq 5.8$. Of course, the actual number of events that were apparently hidden during these periods is rather small. For example, where the fractions are greater

TABLE 2

Fraction of Events Apparently Hidden by Large Earthquakes

M	k	Time Interval (t)	Fraction* (Number) Missed in Ten Years $m_u = 4.0$	$m_u = 4.5$
6.2	96			
		0.5 hr	0.60 (6)	0.36 (9)
		1.0	0.42 (8)	0.27 (14)
		5.0	0.20 (20)	0.08 (20)
6.0	290			
		0.5 hr	0.54 (16)	0.30 (23)
		1.0	0.41 (25)	0.17 (27)
		5.0	0.16 (48)	0.04 (31)
5.8	694			
		0.5 hr	0.40 (29)	0.29 (53)
		1.0	0.18 (26)	0.10 (36)
		5.0	0.12 (87)	0.08 (145)

* 1 - R_c, where R_c is the cumulative ratio plotted in Figure 4 at $m_b = m_u$.

than 0.3, the number missed is no more than 3/year. The reason this number is so small is that large earthquakes are rare, and we expect few earthquakes to occur within hours of them.

Earthquake Swarms

Our results indicate that the detection threshold is usually back to near normal within five hours after large earthquakes. However, there are occasions when swarms of fairly large earthquakes can raise the worldwide network threshold for days, or even weeks. An excellent example of a series of events which had a major effect on the network detection threshold is the Great Sumba earthquake and its aftershocks. The Sumba series began with an m_b 5.7 event at 5:09 GMT on August 8, 1977, and was followed by the m_b 6.4 main shock about one hour later. The main event was located beneath the inner wall of the Java Trench (11.1°S, 118.4°E) at a depth of about 20 km (Fitch et al., 1981) and is believed to be the largest event since the Great Alaskan earthquake of 1964. During the next five days, 61% of the earthquakes in Ringdal's bulletin are aftershocks of the Great Sumba earthquake. In fact, from August 19 to November 30, almost 15% of all earthquakes in the bulletin were located within 1° latitude and longitude of the Sumba main shock. Of the 108 aftershocks occurring within 5 days of the main event, 29 were larger than m_b 5.0.

It is likely that many earthquakes in other parts of the world failed to be detected and cataloged during the Sumba swarm, particularly in the first 5 days. The evidence for this is summarized in Table 3. The 10 year mean and standard deviation for the number of events per 5 day period (excluding periods containing $m_b \geq 6.2$ events) is listed, along with the number of events within and outside the Sumba vicinity during the 5 days after the main shock. For example, we expect to

TABLE 3

Earthquakes Detected During Five Days Following The Great Sumba Earthquake

	$m_b < 4.0$	$m_b < 4.5$	$m_b > 4.5$
Sumba Vicinity	8	51	57
Worldwide (excluding Sumba)	15	44	27
Expected during five days (worldwide)	28.7±10.6*	37.3±17.5	32.6±11.0
Ratio	0.52	0.65	0.83
Confidence that Ratio < 1	90%	90%	70%

*standard deviation

record 28.7 ± 10.6 earthquakes of $m_b < 4.0$ during any 5 day period. However, only 15 such events, or 52% of the expected number, were detected outside of Sumba during 5 days immediately following the main Sumba earthquake. For earthquakes with $m_b < 4.5$, only 65% of the expected number were detected. Thus, for both cases we can say that post-Sumba seismicity was significantly (at the 90% confidence level) below normal outside the Sumba vicinity. While the number of larger ($m_b \geq 4.5$) earthquakes is about 83% of that expected, we cannot say with high confidence that the ratio is significantly less than unity. The examination of the Sumba series demonstrates that there can be extended periods of time during which the network detection threshold is significantly increased.

Discussion

The bulletin used in this study (Ringdal, 1984) provides perhaps the best estimate of current global detection capability, so it is clear from our results that large earthquakes and their aftershock swarms cause small earthquakes to be missed under routine operating conditions. Though the actual number of events apparently missed during short time windows following large earthquakes is small, the fraction of events missed relative to the number expected can be large. These large fractions indicate that an explosion detonated shortly after a large earthquake would have a significantly lower than normal probability of being detected. However,it is difficult to draw firm conclusions about the threat posed by the Hide-in-Earthquake evasion scheme for the following reasons:

1. The statistics are not adequate to give more than a qualitative indication of the increase in the detection threshold caused by large earthquakes. The analysis is hampered by the apparent bias in the m_b of events contributing to F_d, and also by the high threshold of the network. The largest effect on detection capabilities is seen for events with $m_b < 4.5$, but the 90% incremental threshold of the network under normal operating conditions is m_b 4.46.

Thus, even under normal circumstances, only about 40% of the events that actually occur at m_b 4.0 are expected to be detected by this network.

2. There are two ways for small earthquakes to be missed when constructing the bulletin. One is for the event to be missed because the signals are too small to be detected in the coda of the large event. The other is for the event to be missed because of confusion caused by the mixing of P waves from the small earthquake with late arriving phases from the large earthquake. Thus, in many cases the signals from the small events may be detected, but not associated with the proper event. In this connection we note that about 35% of the P wave arrivals reported to the ISC are never associated with an event (R. Adams, ISC, personal communication). We do not know which of these two scenarios is more common. Only the first is considered in most analyses of this problem, (e.g., Evernden, 1976a,b).

3. Explosion signals are usually different from earthquake signals. Our analysis only shows that large earthquakes cause an increase in the threshold for detecting small earthquakes. The threshold for detecting explosions would also increase, but perhaps by a lesser amount.

A conclusive evaluation of the Hide-in-Earthquake evasion scheme is very difficult, perhaps impossible, with bulletin data. Aside from the statistical problems described earlier, we point out that the situation of primary concern, (a small explosion detonated shortly after a large earthquake) simply does not occur often enough (if ever) for conclusions to be drawn. A more thorough analysis of the Hide-in-Earthquake problem requires some simulations. These can be done in two ways. One is by constructing synthetic seismograms, most realistically by summing recordings of earthquakes and explosions. This is an excellent way to study station detection threshold effects, but it is difficult to simulate the full network performance this way. There are

computer programs that simulate network performance and calculate the detection threshold (e.g., Wirth, 1970). But these programs require a variety of seismological assumptions, and the results are only credible if they have been carefully normalized to actual network performances. Ringdal (1984) was able to simulate the normal detection performance of the 115 station network studied here. If the simulation program is realistic, it should also be able to simulate the effect of the large earthquakes documented here. Thus, the data in Figure 2 provide a severe test for the simulation models. A successful simulation of these data would provide a very credible basis for simulating the hypothetical hide-in-earthquake scenarios of primary concern for monitoring a test ban treaty.

Conclusions

The results summarized in Table 2 and Figure 6 indicate that the detection capability of the 115 station global network defined by Ringdal (1984) is significantly degraded for periods up to an hour or so after earthquakes as small as m_b 5.8. Also, the Table 3 data for the Great Sumba earthquake and its aftershocks indicate that earthquake swarms can disturb the network detection threshold for periods of days and even weeks. Both results indicate that events with magnitude less than 4.5 have a significantly smaller probability of being detected if they occur shortly after a large earthquake. However, it is difficult to use these results to justify conclusions about the effectiveness of the Hide-In-Earthquake evasion scheme. This can best be done with network simulation models, but the results of this paper provide a basis for normalizing such models to actual network performances.

REFERENCES

Blandford, R.R. (1977). Discrimination between earthquakes and under ground explosions, Ann. Rev. Earth Planet Sci., 5, 111-122.

Burnetti, J.A. and D.W. Rivers (1984). Hide-in-earthquake evasion studies using breadboard data. TGAL-TR-84-5, Teledyne Geotech, Alexandria, Virginia.

Evernden, J.F. (1976a). Study of seismological evasion. Part I. General discussions of various evasion schemes. Bull. Seis. Soc. Am. 66, 245-280.

Evernden, J.F. (1976b). Study of seismological evasion. Part III. Evaluation of evasion possibilities using codas of large earthquakes, Bull. Seis. Soc. Am. 66, 549-592.

Filson, J.R. (1973). On estimating the effect of Asian earthquake codas on the explosion detection capability of LASA, Technical Report 1973-29, Lincoln Laboratory, Massachussetts Institute of Technology, Lexington, MA.

Fitch, T.J., R.G. North, and M.W. Shields (1981). Focal depths and moment tensor representations of shallow earthquakes associated with the Great Sumba earthquake, J. Geophys. Res., 86, 9357-9374.

Ringdal, F. (1976). Maximum-likelihood estimation of seismic magnitude, Bull. Seism. Soc. Am. 66, 789-802.

Ringdal, F. (1978). A reply to "Comments on the use of truncated distribution theory for improved magnitude estimation," by D. von Seggern and D.W. Rivers, Bull. Seism. Soc. Am., 68, 1547-1548.

Ringdal, F. (1984). Study of magnitudes, seismicity and earthquake detectability using a global network, NORSAR Semi-annual Technical Summary 10 Oct. 1983 - 31 Mar. 1984, Kjeller, Norway.

Wirth, M.H. (1970). Estimation of network detection and location capability, Air Force Technical Applications Center, Washington, D.C.

Von Seggern, D. and D.W. Rivers (1978). Comments on the use of truncated distribution theory for improved magnitude estimation, Bull. Seism. Soc. Am., 68, 1543-1546.

END

FILMED

4-86

DTIC